AMERICAN SOCIETY FOR MICROBIOLOGY | Journal of Virology®

VIRUS-CELL INTERACTIONS

Identification of Cellular Genes Involved in Baculovirus GP64 Trafficking to the Plasma Membrane

Jeffrey J. Hodgson,[a] Nicolas Buchon,[b] Gary W. Blissard[a]

[a]Boyce Thompson Institute at Cornell University, Ithaca, New York, USA
[b]Department of Entomology, Cornell University, Ithaca, New York, USA

Nicolas Buchon and Gary W. Blissard contributed equally to this article as co-senior authors. Senior author order was determined by order of increasing seniority.

ABSTRACT The baculovirus envelope protein GP64 is an essential component of the budded virus and is necessary for efficient virion assembly. Little is known regarding intracellular trafficking of GP64 to the plasma membrane, where it is incorporated into budding virions during egress. To identify host proteins and potential cellular trafficking pathways that are involved in delivery of GP64 to the plasma membrane, we developed and characterized a stable *Drosophila* cell line that inducibly expresses the AcMNPV GP64 protein and used that cell line in combination with a targeted RNA interference (RNAi) screen of vesicular protein trafficking pathway genes. Of the 37 initial hits from the screen, we validated and examined six host genes that were important for trafficking of GP64 to the cell surface. Validated hits included Rab GTPases *Rab1* and *Rab4*, *Clathrin heavy chain*, clathrin adaptor protein genes *AP-1-2β* and *AP-2μ*, and *Snap29*. Two gene knockdowns (*Rab5* and *Exo84*) caused substantial increases (up to 2.5-fold) of GP64 on the plasma membrane. We found that a small amount of GP64 is released from cells in exosomes and that some portion of cell surface GP64 is endocytosed, suggesting that recycling helps to maintain GP64 at the cell surface.

IMPORTANCE While much is known regarding trafficking of viral envelope proteins in mammalian cells, little is known about this process in insect cells. To begin to understand which factors and pathways are needed for trafficking of insect virus envelope proteins, we engineered a *Drosophila melanogaster* cell line and implemented an RNAi screen to identify cellular proteins that aid transport of the model baculovirus envelope protein (GP64) to the cell surface. For this we developed an experimental system that leverages the large array of tools available for *Drosophila* and performed a targeted RNAi screen to identify cellular proteins involved in GP64 trafficking to the cell surface. Since viral envelope proteins are often critical for production of infectious progeny virions, these studies lay the foundation for understanding how either pathogenic insect viruses (baculoviruses) or insect-vectored viruses (e.g., flaviviruses, alphaviruses) egress from cells in tissues such as the midgut to enable systemic virus infection.

KEYWORDS vesicular protein trafficking, *Drosophila*, AcMNPV, high-throughput screen, baculovirus, viral envelope protein

For enveloped viruses, viral envelope proteins are typically essential for virus entry, playing roles in receptor recognition, binding, and membrane fusion. They may also play critical roles in assembly and production of infectious progeny virions. Virus assembly is a complex process that varies dramatically among different virus groups, depending on the subcellular replication site and strategy utilized for assembly and egress. During replication and assembly, cellular protein transport pathways are critical for delivering viral components to the appropriate subcellular compartments or

Editor Rozanne M. Sandri-Goldin, University of California, Irvine

Address correspondence to Gary W. Blissard, gwb1@cornell.edu, or Nicolas Buchon, nicolas.buchon@cornell.edu.

The authors declare no conflict of interest.

Received 28 January 2022
Accepted 31 March 2022
Published 24 May 2022

locations where processes such as budding and egress occur (1). This is especially true for viral envelope proteins, which must associate with newly assembled nucleocapsids and/or other viral and cellular factors during the assembly process.

Because different viruses have an assortment of replication and release strategies, the transport of viral envelope proteins to the appropriate sites of viral particle assembly and egress can involve a variety of vesicular protein transport pathways. The virus *Autographa californica multiple nucleopolyhedrovirus* (AcMNPV) has a well-studied envelope protein, GP64, that is critical for virion entry and is important for the production of the budded virus (BV) morphotype (2). Production of baculovirus BVs begins when AcMNPV capsids package the viral genome in the nucleus and the resulting nucleocapsids are transported out of the nucleus by a process that involves actin-mediated propulsion (3). Nucleocapsids then transit to the plasma membrane and bud there, acquiring the GP64 envelope glycoprotein in the final step of the BV assembly process.

To begin to understand how the GP64 envelope protein is trafficked to the plasma membrane, we have examined the trafficking of GP64 in cultured insect cells. For these studies, we developed an assay based on inducible GP64 expression in a stable cell line and performed quantitative measurements of the GP64 protein on the cell surface when expression of a single cellular gene was disrupted. This experimental system permits high-throughput screening and identification of host proteins required for GP64 trafficking to the plasma membrane. We used cultured *Drosophila* cells, which produce robust RNAi responses following incubation with double-stranded RNAs (dsRNAs) and have a well-studied genome with readily available resources for interrogating specific pathways or the whole genome (4). Thus, for the current study, we generated a *Drosophila* cell line that expresses the AcMNPV GP64 protein in an inducible manner and performed an RNA interference (RNAi) screen targeting a wide variety of genes known to be involved in or associated with vesicular protein transport. Integral membrane proteins such as GP64 are transported from the Golgi to the plasma membrane (PM) via small vesicles and a variety of interconnected endosomal pathways. We found that single-gene knockdowns of 6 genes (Rab GTPases *Rab1* and *Rab4*, *Clathrin heavy chain*, clathrin adapter protein genes *AP-1-2*β and *AP-2*μ, and *Snap29*) each resulted in significantly reduced GP64 transport to and/or maintenance of GP64 on the cell surface. In addition, we identified two gene knockdowns (*Rab5* and *Exo84*) that each resulted in substantial increases in levels of cell surface GP64. Based on the predicted functional roles of Rab4, AP-2μ, and Rab5 in membrane protein recycling from the cell surface, we also examined the potential for GP64 recycling. We found that GP64 was endocytosed from the cell surface and that it was internalized and delivered to VPS26 (retromer) containing endosomes, suggesting that the endocytosed GP64 may be recycled back to the plasma membrane.

RESULTS

Generation of a *Drosophila* cell line expressing GP64. To begin to understand the roles of cellular proteins and pathways in trafficking of the baculovirus envelope glycoprotein GP64 to the plasma membrane in insect cells, we engineered a *Drosophila* cell line to inducibly express GP64 and used that cell line for a targeted RNAi screen of host genes associated with vesicular protein trafficking of membrane proteins (Fig. 1A and B and 2). First, *Drosophila* DL1 cells that inducibly express the baculovirus GP64 envelope protein were generated by cotransfecting DL1 cells with two plasmids, one encoding the WT AcMNPV GP64 protein under the control of the inducible *Drosophila melanogaster metallothionein* promoter and a second containing a puromycin resistance gene under the control of a constitutive *D. melanogaster copia* promoter. Following transfection, cells were selected on puromycin, then GP64 expression was induced by addition of Cu_2SO_4 to the medium. Cells displaying GP64 at the cell surface were identified by immunolabeling (with an anti-GP64 monoclonal antibody) cells at 4°C, and single cells identified as expressing GP64 were isolated by fluorescence-activated cell sorting (FACS) and single-cell cloned. A clonal cell line that inducibly expresses GP64 was named DL1:mtGP64. DL1:mtGP64 cells

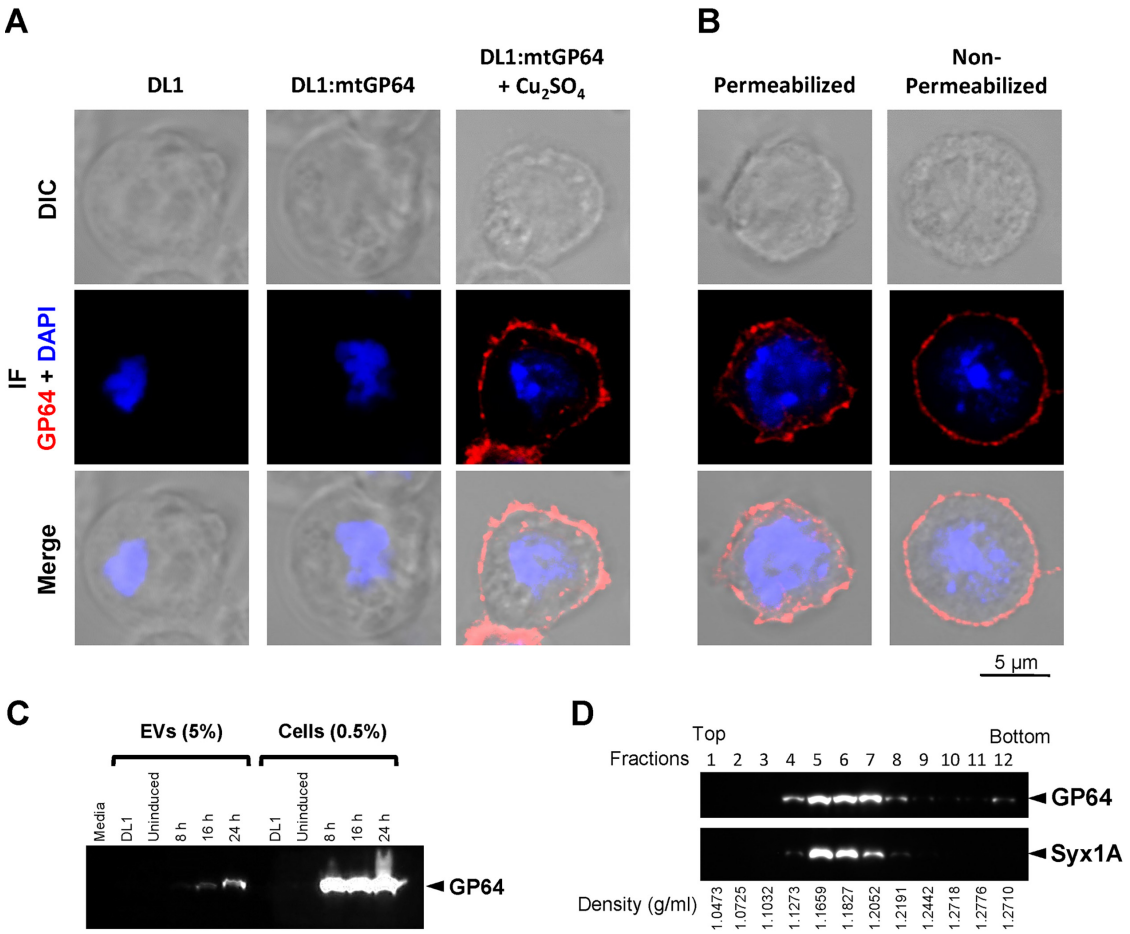

FIG 1 Inducible expression and localization of GP64 in DL1:mtGP64 cells, a stable *Drosophila* cell line that inducibly expresses GP64. (A) GP64 immunostaining (red) in DL1 or DL1:mtGP64 cells, either untreated or treated with copper ($+Cu_2SO_4$) to induce GP64 expression. Cells were permeabilized with Triton X-100 for detection of total cellular GP64. DIC, differential interference contrast; IF, immunofluorescence; DAPI, nuclear staining. (B) Comparison of total cell GP64 versus cell surface GP64 in permeabilized and nonpermeabilized DL1:mtGP64 cells, respectively. (C) Comparison of relative levels of GP64 in DL1:mtGP64 cells with that in EVs. At various times (8, 16, and 24 h) following Cu_2SO_4 induction of GP64 expression, cellular GP64 was compared with GP64 from EVs isolated from growth medium, by SDS-PAGE and immunoblotting. For each time point, 5% of each EV preparation was compared with 0.5% of each total cell protein preparation (see Materials and Methods). DL1 cells (DL1) and uninduced DL1:mtGP64 cells (Uninduced) were also included as controls. (D) EVs collected from DL1:mtGP64 cell supernatant at 24 h after Cu_2SO_4 induction were fractionated in a sucrose gradient, and fractions were analyzed on immunoblots. GP64 and syntaxin 1A (Syx1A, a marker of exosomes) were identified using monoclonal anti-GP64 AcV5 and anti-Syx1A Ab ID 528484 (DSHB) antibodies, respectively. For all panels, cells were induced by treatment with 200 μM Cu_2SO_4.

were further examined to verify efficient trafficking of GP64 to the plasma membrane (Fig. 1A and B). DL1:mtGP64 cells did not express detectable GP64 in the absence of Cu_2SO_4 induction, but GP64 was detected on the surface of cells after 8 h of incubation in Cu_2SO_4 (Fig. 1A; DL1:mtGP64 versus DL1:mtGP64$+Cu_2SO_4$).

GP64 traffics predominantly to the surfaces of DL1 cells. Comparisons of GP64 detected from nonpermeabilized and permeabilized cells (Fig. 1B) indicated that the majority of GP64 was trafficked to and displayed on the cell surface, while relatively little GP64 was detected in transit. Because some viral envelope proteins are also released from the cell in extracellular vesicles (EVs) (5–10), we examined the potential for GP64 release from the cell via EVs. We first compared relative levels of GP64 detected in EVs versus whole cells after 8, 16, and 24 h of copper-induced GP64 expression. EVs in the culture supernatant were isolated by low-speed centrifugation to remove cells and cell debris, followed by pelleting through a 25% sucrose cushion. GP64 in the EV fraction was then compared to that in whole-cell lysates at each time point (Fig. 1C). While GP64 was detected in the EV fraction from cell culture supernatant, cellular GP64 levels appeared to be >100-fold higher

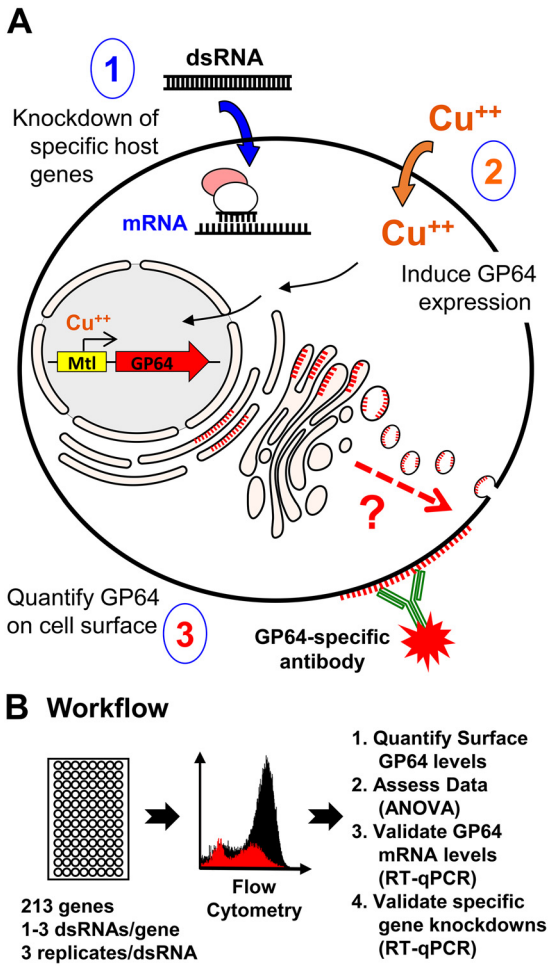

FIG 2 Overview and workflow of an RNAi screen using the DL1:mtGP64 cell line. (A) Schematic of RNAi knockdowns, induction of GP64 expression, and quantification of cell surface GP64. (Step 1) Cells in wells of a 96-well plate were incubated in gene-specific (or nonspecific *lacZ* control) dsRNA-containing growth medium (without copper) for 4 days. (Step 2) Copper (Cu_2SO_4) was then added to cells to induce GP64 expression for 8 h. (Step 3) Surface levels of GP64 were determined on ice-chilled monolayers of live cells by immunostaining with a phycoerythrin-conjugated GP64 antibody and quantification by flow cytometry. (B) Each assay plate contained 54 wells containing individual test dsRNAs, 3 wells containing *lacZ* (negative-control) dsRNA, and 3 wells containing Rab1-specific (positive-control) dsRNA. Relative abundance of cell surface GP64 staining was assessed by flow cytometry, based on the geometric means of fluorescence detected for each gene-specific (test) dsRNA compared to that of both the control *lacZ* dsRNA treated cells and the average of all 54 test wells in each plate. The effect of each dsRNA was assessed statistically from triplicate independent experiments (ANOVA). Hits were validated first by measuring *gp64* mRNA levels (RT-qPCR) to eliminate effects on *gp64* gene expression and then by measuring specific target gene knockdown efficiency (RT-qPCR).

than that from the culture supernatant EVs (Fig. 1C, EVs versus Cells), based on estimates from Western blots. We next examined the type of extracellular vesicle (i.e., microvesicles or exosomes) that contained the extracellular GP64. EVs from the cell culture supernatant were analyzed by pelleting through a 25% sucrose cushion, followed by fractionation on a sucrose gradient. Our results indicate that extracellular GP64 was found in exosomes, since the distribution of GP64 in the gradient was coincident with that of syntaxin 1A, a protein enriched in exosomes (11, 12) (Fig. 1D). Extracellular GP64 cofractionated with syntaxin 1A in sucrose densities of 1.1659 to 1.2052 g/L, densities in which exosomes are typically recovered (13). We did not further assess whether GP64 was present in larger, plasma membrane-derived microvesicles, so it is unclear whether GP64 may also be released from cells in that manner. Overall, these results show that the majority of GP64 expressed in the

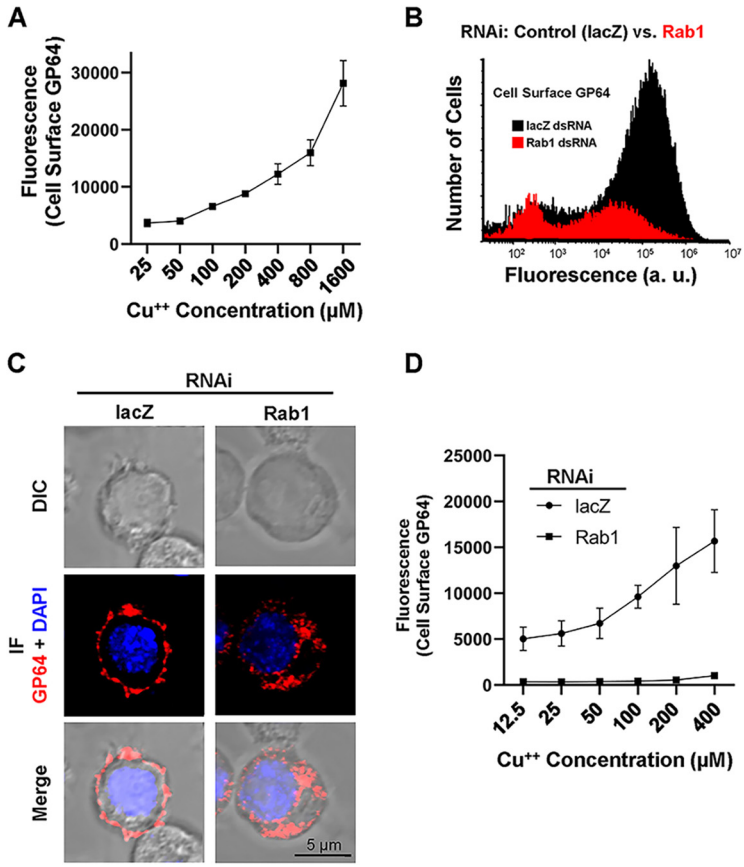

FIG 3 Optimization of GP64 expression and RNAi sensitivity. The effects of Cu_2SO_4 dose on GP64 induction and cell surface localization were analyzed in the presence of an RNAi knockdown. (A) Relative cell surface GP64 levels (determined by flow cytometry of DL1:mtGP64 cells) were determined following incubation for 8 h in increasing doses (25 to 1,600 μM) of Cu_2SO_4, as described in Materials and Methods. (B) Flow cytometry data showing differential GP64 cell surface levels on cells treated with dsRNA targeting *Rab1* (red) or negative control *lacZ* (black) for 4 days. (C) Distribution of GP64 in cells treated with *Rab1*-specific or negative control *lacZ* dsRNA. After 4 days of dsRNA exposure, cells were seeded on coverslips and induced with 200 μM Cu_2SO_4 for 16 h, then permeabilized with Triton X-100, and immunostained for GP64 (red). (D) Comparisons and optimization of the effects of a Rab1 knockdown on cell surface GP64 levels. Cells exposed to Rab1 or *lacZ* dsRNA for 4 days were induced for 8 h with increasing concentrations (12.5 to 400 μM) of Cu_2SO_4, and then levels of cell surface GP64 were determined by flow cytometry. For panels A and D, the GP64 surface levels (geometric means) of cells treated with Rab1 or *lacZ* dsRNA were determined by flow cytometry. The data in panels A and D are the averages from 5 individual wells of cells treated with each dsRNA and induced with each dose of Cu_2SO_4. Error bars indicate standard deviations from the mean.

cell is trafficked to the plasma membrane and that only a minor fraction of GP64 exits the cell by exocytosis.

Optimization of GP64 cell surface levels for detecting the effects of host gene knockdowns. The strategy and workflow of experiments to identify cellular factors involved in GP64 trafficking to the cell surface are illustrated in Fig. 2. To maximize sensitivity in identifying quantitative changes in GP64 surface levels resulting from trafficking defects from host gene knockdowns (Fig. 2A), GP64 cell surface levels should be measured at a relatively early time following induction and should be robust but not saturating. Because relatively robust GP64 surface levels were detected at 8 h postinduction in our preliminary studies, we optimized induction and the effects of RNAi knockdowns at that time point. First, GP64 surface levels were measured after 8 h of incubation in increasing concentrations of Cu_2SO_4 (Fig. 3A). We identified Cu_2SO_4 concentrations (100 to 800 μM) that resulted in GP64 surface levels that were robust but not saturating and were within a linear range of the dose-response curve. This range of Cu_2SO_4 concentrations elicited increasing levels of detectable

TABLE 1 Genes screened for effects on GP64 trafficking

Gene group (no. screened)	Genes screened
ARF GTPases (15)	*plx*, *sar1*, *arf51*, *arf79F*, *arf102F*, *arl1*, *arl2*, *arl4*, *arl5*, *arl6*, *dnd*, *gie*, *cg4789*, *sec23*, *arfrp1*
ARF effectors (9)	*ArfGAP1*, *CenG1A*, *drongo*, *ArfGAP3*, *Asap*, *CG8243*, *CenB1A*, *Git*, *RhoGAP15B*
RAB GTPases (34)	*Rab1 Rab2*, *Rab3*, *Rab4*, *Rab5*, *Rab6*, *Rab7*, *Rab8*, *Rab9*, *Rab9Db*, *Rab9Fa*, *Rab9Fb*, *Rab10*, *Rab11*, *Rab14*, *Rab18*, *Rab19*, *Rab20*, *Rab21*, *Rab23*, *Rab26*, *Rab27*, *Rab29*, *Rab30*, *Rab32*, *Rab35*, *Rab39*, *Rab40*, *RabX1*, *RabX2*, *RabX4*, *RabX5*, *RabX6*
RAB effectors/TRAPP (47)	*Trs33*, *Trs31*, *Trs85*, *Syx7*, *Trs20*, *Trs23*, *l(3)76BDm*, *Bet5*, *brun*, *Bet3*, *SIDL*, *Trs31*, *CG9067*, *gry*, *Mon1*, *Ccz1*, *CG18659*, *Crag*, *pns*, *Sbf*, *Rab3-GEF*, *strat*, *ca*, *CG7324*, *CG31935*, *TBC1D5*, *sky*, *CG1695*, *CG7742*, *CG17883*, *CG5745*, *Tbc1d15-17*, *RN-tre*, *GAPcenA*, *CG42795*, *CG5916*, *CG8155*, *Evi5*, *CG6182*, *GAPsec*, *CG4041*, *TBC1D16*, *CG4552*, *wkd*, *CG12241*, *CG16896*, *CG32506*
Kinesins (25)	*cana*, *CG10845*, *CG14535*, *cmet*, *cos*, *Khc*, *Khc-73*, *Kif3C*, *Klp3A*, *Klp10A*, *Klp31E*, *Klp54D*, *Klp59C*, *Klp59D*, *Klp61F*, *Klp64D*, *Klp67A*, *Klp68D*, *Klp98A*, *ncd*, *neb*, *nod*, *pav*, *sub*, *unc-104*
Exocyst (8)	*Sec3*, *Sec5*, *Sec6*, *Sec8*, *Sec10*, *Sec15*, *Exo70*, *Exo84*
ESCRT (14)	*Vps2*, *Vps2b. Vps22*, *Vps23*, *Vps24*, *Vps25*, *Vps27*, *Vps28*, *Vps32*, *Vps36*, *Vps37B*, *Vps60*, *Chmp1*, *stam*
VPS (21)	*Vps1*, *Vps4*, *Vps13*, *Vps13B*, *Vps13D*, *Vps15*, *Vps16B*, *Vps18*, *Vps20*, *Vps33A*, *Vps33B*, *Vps34*, *Vps38*, *Vps41*, *Vps45*, *Vps51*, *Vps52*, *Vps53*, *Vps54*, *Vps74*, *Vta1*
Retromer (3)	*Vps26*, *Vps29*, *Vps35*
Clathrin/AP (14)	*Chc*, *Clc*, *AP-1*γ, *AP-1*μ, *AP-1*σ, *AP-1-2*β, *AP-2*α, *AP-2*μ, *AP-2*σ, *cm*, *g*, *or*, *rb*, *gga*
P24 transporters (8)	*eclair*, *CG33105*, *emp24*, *CG9308*, *baiser*, *CG1967*, *CG31787*, *logjam*
COP (9)	*sec24CD*, *sec23*, α*COP*, β*'COP*, β*COP*, δ*COP*, ε*COP*, ζ*COP*, γ*COP*
COG (8)	*Cog1*, *ldlCp*, *Cog3*, *CG7456*, *fws*, *CG1968*, *Cog7*, *CG6488*

GP64, while concentrations above 800 μM resulted in less consistent levels of GP64 induction and/or detection.

To optimize the assay for measuring the effects of RNAi knockdowns, we next measured GP64 surface levels resulting from increasing concentrations (12.5 to 400 μM) of Cu_2SO_4, in the presence of an RNAi knockdown (Fig. 3B to D). For the RNAi knockdown, we selected Rab1 as a positive control for inhibition of trafficking to the cell surface. Rab1 is important for regulating vesicular protein trafficking from the endoplasmic reticulum (ER) to the Golgi compartment (14), and the Rab1 knockdown should therefore inhibit protein trafficking to the cell surface. As expected, we found that dsRNA-mediated knockdown of Rab1 in DL1:mtGP64 cells, followed by induction of GP64 expression by Cu_2SO_4, resulted in dramatically lower levels of cell surface GP64, compared with negative-control cells treated with *lacZ* dsRNA (Fig. 3B). Typical cell surface localization of GP64 was observed for the control *lacZ* dsRNA-treated cells but was disrupted in cells with the Rab1 knockdown (Fig. 3C, *lacZ* versus Rab1). To optimize the detection of the effects of RNAi knockdowns on GP64 trafficking, we next examined the effect of a Rab1 knockdown in the context of various concentrations of Cu_2SO_4 (12.5 to 400 μM). By comparisons to RNAi knockdowns with the negative-control *lacZ* dsRNA, we identified a range of Cu_2SO_4 concentrations (50 to 400 μM) that resulted in substantial GP64 cell surface differences between the Rab1 knockdown and the negative control (*lacZ*) (Fig. 3D). Thus, these conditions provide a sensitive measure of the effect of the Rab1 RNAi knockdown on GP64 surface levels. Based on the differential effects of negative-control *lacZ* and positive-control Rab1 knockdowns on GP64 cell surface detection, we calculated a Z-factor of 0.67 for our assay (Z-factors between 0.5 and 1.0 signify an excellent high-throughput assay for detecting hits [15]), indicating that the assay parameters we developed are capable of identifying gene knockdowns that modulate GP64 trafficking and surface display. We therefore based our RNAi screen (see below) on these induction parameters established using Rab1.

Overview of screen results. To identify genes and pathways necessary for GP64 trafficking to the cell surface, we selected 213 cellular genes for dsRNA knockdowns in this targeted RNAi screen. Families of genes examined in the screen included members of approximately 13 groups of genes associated with membrane protein trafficking (Table 1). For RNAi knockdowns of each gene, up to 3 unique gene regions (containing no identified off-target effects) were selected for generation of dsRNAs. This resulted in a total of 561 dsRNAs in each replicate of the RNAi knockdown experiment (see Table S2 in the supplemental material), which was performed 3 times (3 biological replicates).

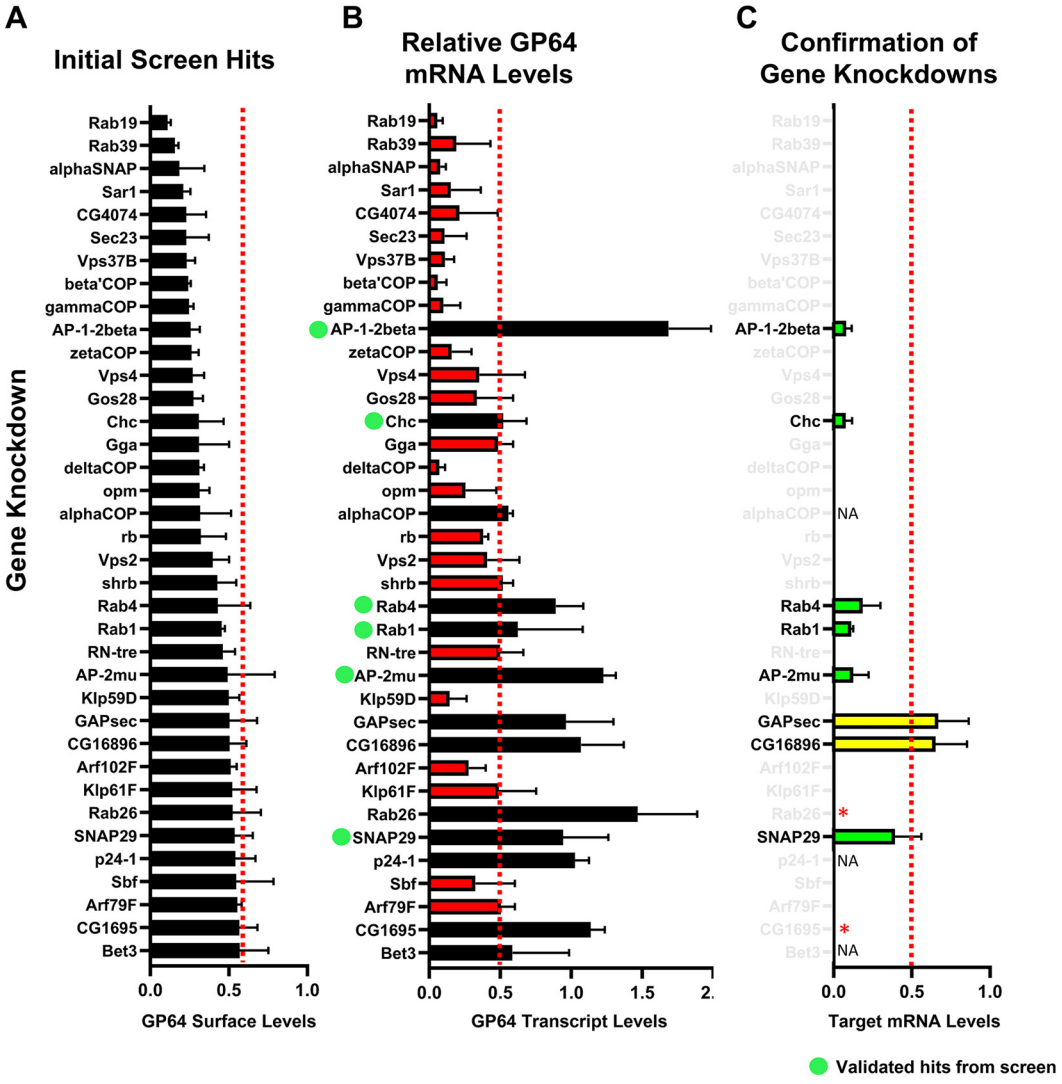

FIG 4 Identification of genes important for transport of GP64 to the cell surface. (A) The targeted RNAi screen of 213 *Drosophila* genes identified 37 gene knockdowns that reduced GP64 cell surface levels by 40% or more. Gene names are indicated on the left, and bars indicate GP64 surface levels relative to the knockdown by control *lacZ* dsRNA. The dashed red line indicates 60% of the control dsRNA knockdown. (B) Analysis of *gp64* mRNA levels. For each of the indicated host gene knockdowns, *gp64* mRNA levels were quantified by RT-qPCR and compared with *gp64* mRNA levels of the negative control (*lacZ* dsRNA, 1.0). (C) Confirmation of target host gene knockdowns. Gene-specific mRNA knockdown levels for selected target host genes were determined by RT-qPCR and compared with that from knockdown of the negative control (*lacZ* dsRNA, 1.0). NA, not analyzed. *, not expressed. In panels B and C, the dashed red lines indicate 50%.

We used the following method to identify genes as hits for our immediate follow-up analysis. Genes were selected as hits when a knockdown resulted in significantly lower GP64 surface levels relative to 2 controls: (i) the *lacZ* knockdown controls on each assay plate and (ii) the average value from all wells on each assay plate.

From the 213 genes targeted in the RNAi screen, 37 gene knockdowns resulted in GP64 surface levels that were reduced by ≥40% compared with the controls. The 37 knockdowns (Fig. 4A; Table S3) included genes encoding 4 Arf GTPases, 3 ESCRT proteins, 10 clathrin/adaptor proteins, 2 kinesins, 2 P24 transporters, 5 RAB GTPase effectors, 5 RAB GTPases, 2 SNARE proteins, 1 SNAP protein, and 3 VPS proteins.

Validation of genes required for GP64 transport to the plasma membrane. (i) qPCR analysis of GP64 mRNA. In addition to direct effects of knockdowns on protein transport, reduced GP64 surface levels from some knockdowns could have resulted from indirect effects on other cellular systems affecting *gp64* gene expression. Therefore, to determine whether some knockdowns affected *gp64* gene expression, we examined *gp64*

transcript levels. For each of the 37 hits (Fig. 4A; Table S3), we used reverse transcription-quantitative PCR (RT-qPCR) to quantify GP64 transcript levels following RNAi knockdown of the target host gene and Cu_2SO_4 induction of GP64 expression. The analysis of *gp64* transcript levels revealed that *gp64* transcripts were substantially affected (reduced to ≤50%) for 24 of the 37 gene knockdowns (Fig. 4B, red bars), indicating indirect effects on GP64 expression. The remaining 13 gene knockdowns (Fig. 4B, black bars) had *gp64* transcript levels exceeding 50% of that in the control knockdown (*lacZ*). Ten of these genes (*Rab1*, *Rab4*, *Rab26*, *GAPsec*, *CG16896*, *CG1695*, *Snap29*, *Chc*, *AP-1-2*β, and *AP-2*μ) were selected for further analysis, in part because they resulted in the most severely depleted cell surface GP64 levels and also due to their importance in Golgi-to-PM transport of integral membrane proteins.

(ii) Confirmation of cellular gene mRNA knockdowns. To verify the knockdown of mRNAs of each of the 10 candidate cellular genes, we used RT-qPCR to confirm the depletion of each of the target mRNAs by dsRNA-mediated RNAi. Of these 10 knockdowns, we verified the mRNA knockdown for 6 genes (Fig. 4C, green bars). Assessments of mRNA levels for two of these genes (*Rab26* and *CG1695*) were difficult in both control *lacZ* dsRNA-treated cells and Rab26 and CG1695 dsRNA-treated cells. Our results suggested that neither of these genes was expressed in our DL1-derived cell line (Fig. 4C, asterisks), and modENCODE cell line expression data available at the Drosophila Genomics Resource Center indicate that neither gene is expressed in DL1 (also called S1) or many other *Drosophila* cell lines (https://dgrc.bio.indiana.edu/cells/TilingSearch). The dsRNA knockdowns of *GAPsec* and *CG16896* resulted in a reduction of only approximately 30% relative to control mRNA levels (Fig. 4C, yellow bars). While this modest knockdown level may be responsible for the modest reduction in GP64 transport, we did not further examine these genes. Therefore, we considered the 6 remaining gene knockdowns that resulted in more dramatic mRNA depletions (Fig. 4C, green bars). The 6 gene knockdowns that were fully validated in reducing GP64 trafficking to the cell surface included genes encoding 3 clathrin adaptor proteins or clathrin (AP-1-2β, AP-2μ, and Chc [clathrin heavy chain]), 2 Rab GTPase proteins (Rab1 and Rab4), and a SNAP protein associated with vesicular trafficking (Snap29) (Fig. 4C).

Microscopic analysis of GP64 localization in cells with each of the 6 validated gene knockdowns. Our flow cytometry-based RNAi screen identified 37 gene knockdowns (hits) that resulted in substantially reduced GP64 levels at the cell surface. By eliminating hits that may have resulted from indirect effects (pleiotropic effects on *gp64* transcription or mRNA levels or effects on nontarget genes), we subsequently narrowed the validated hits to a subset of 6 gene knockdowns. To further detail the effects of these knockdowns, we used confocal microscopy to examine the localization of GP64 following knockdown of each of the 6 identified genes (Fig. 5). To identify GP64 accumulation in organelles or cellular compartments following these target gene knockdowns, we immunostained GP64 and counterstained for markers of a variety of cellular compartments. Specific antibodies or reagents were used to identify the following compartments (by specific marker proteins): plasma membrane (concanavalin A), nuclear envelope (lamin A), endoplasmic reticulum (calnexin 99A), Golgi apparatus (golgin 245 and Golgi microtubule-associated protein), retromer (VPS26), recycling endosomes (Rab11), late endosomes (Rab7), and lysosomes (cathepsin L). For studies of GP64 accumulation, GP64 localization was examined in the presence of each of the 6 knockdowns and compared with GP64 localization in control cells treated with *lacZ* dsRNA. As with untreated cells (Fig. 1A and B), we found that GP64 was localized predominately at the plasma membrane in control cells treated with *lacZ* dsRNA (Fig. 5, *lacZ*). Only small amounts of GP64 were detected in the perinuclear region and in a few very small, faint cytoplasmic puncta in the control cells. For cells with knockdowns from each of the 6 hits in the screen, we confirmed the substantial reductions of GP64 at the plasma membrane (Fig. 5, LacZ versus Chc, AP-1-2β, AP-2μ, Rab1, Rab4, and Snap29). Furthermore, we identified substantial intracellular GP64-specific staining, implying that GP64 accumulation in cellular compartments was due to dysregulated trafficking.

Clathrin-related gene knockdowns. Clathrin-coated vesicles (CCVs) produced from the trans-Golgi network (TGN), from endosomes or at the plasma membrane are each

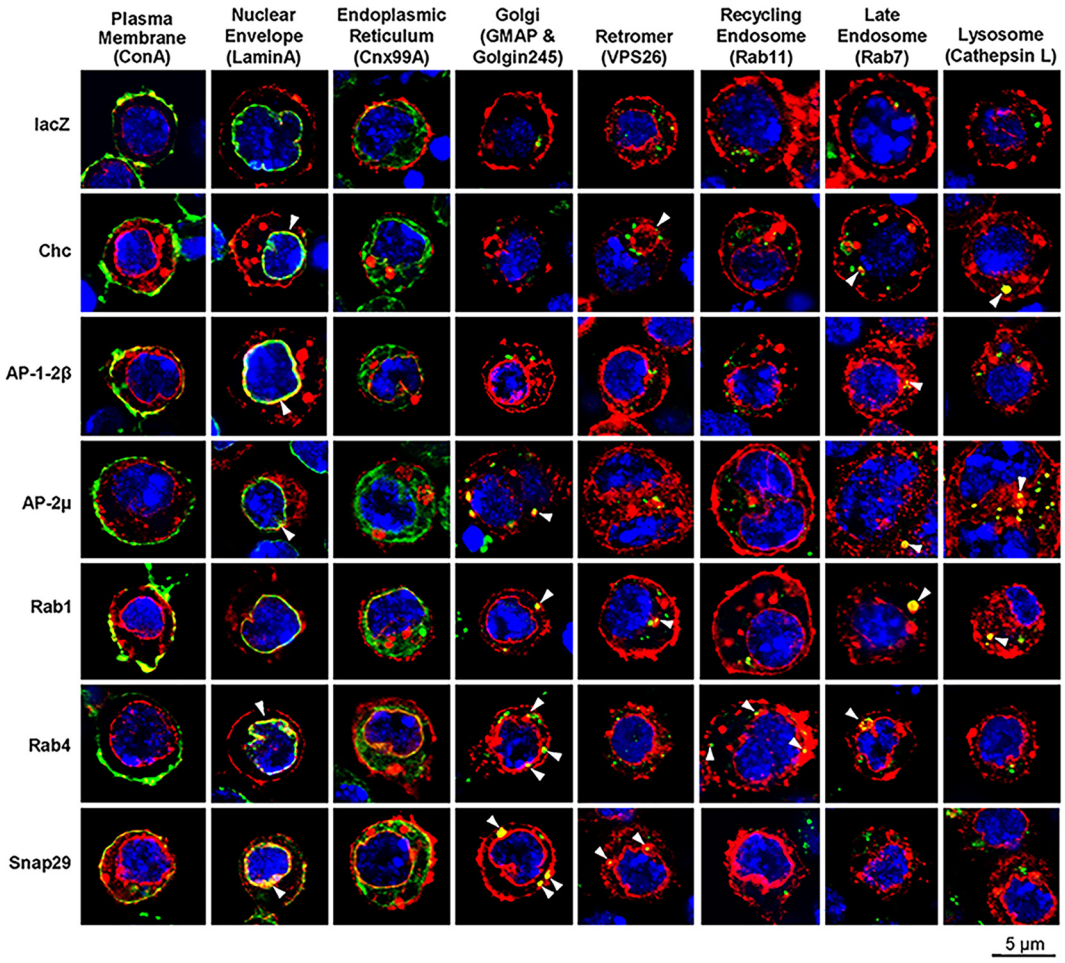

FIG 5 Cellular localization of GP64 in cells with RNAi knockdowns of validated target genes. Cells were exposed to each indicated dsRNA for 4 days and then seeded onto sterile coverslips. GP64 expression was induced by incubation in 200 μM Cu_2SO_4 for 16 h. Cells were permeabilized with Triton X-100 and costained for GP64 (red), DAPI (blue), and the indicated organelle protein markers (green) and imaged with a 63× oil immersion objective of a confocal microscope. RNAi knockdowns are indicated on the left of each row, and cellular compartment marker staining is indicated above each column. Examples of colocalization of GP64 with compartment-specific markers are indicated by arrowheads.

involved in distinct trafficking routes (16, 17). The coat proteins (clathrin light and heavy chains) form triskelions that themselves do not bind directly to lipid bilayers. Rather, they require accessory proteins (adaptor proteins) to be recruited to specific organelle membranes (18–21) and therefore dictate the composition and location of distinct CCVs (22). Each CCV subtype is composed of four discrete adaptor protein subunits (19–21), which provides specificity to the CCV protein complexes, likely because CCVs are used in many different trafficking routes among several organelles. The adaptor proteins (adaptins) are involved in recruiting cargo proteins (e.g., GP64) into their vesicles. In the current study, knockdown of *clathrin* and related adaptin genes (*Chc*, *AP-1-2*β, and *AP-2*μ) resulted in severely depleted GP64 cell surface levels (Fig. 4A) while *gp64* mRNA levels were either increased (*AP-1-2*β and *AP-2*μ) or only moderately reduced (*Chc*) (Fig. 4B). For knockdowns of *Chc*, *AP-1-2*β, and *AP-2*μ, we detected a substantial accumulation of GP64 in the perinuclear area and also frequently in large cytoplasmic puncta. GP64 accumulation appeared most notable for the knockdown of *Chc* (Fig. 5; LacZ versus Chc, AP-1-2β, and AP-2μ). The perinuclear GP64 accumulation colocalized with the nuclear envelope marker (lamin A), indicating accumulation in the nuclear envelope when expression of clathrin or clathrin adaptors was disrupted. Cytoplasmic accumulation of GP64 (large puncta) was observed colocalized with Golgi (golgin 245), lysosome (cathepsin L), and late-endosome (Rab7) markers, suggesting that clathrin and related adaptors are involved at different levels of

GP64 intracellular trafficking. Cells with a *Chc* knockdown often contained bright GP64 ring-shaped puncta decorated with several adjacent retromer/VPS26-stained puncta, highlighting the idea that GP64 trafficking is likely stalled in endosomes due to disruption of CCV assembly, tethering, and/or GP64 cargo recruitment.

Rab knockdowns. Rab GTPases are important regulators of vesicular transport, and many Rab GTPases (and Rab effectors) were identified in the 37 hits initially identified from the RNAi screen. Following further analysis and validation by monitoring *gp64* mRNA levels and target gene mRNA knockdown efficiencies, we narrowed the hits to 2 Rab GTPases, Rab1 and Rab4. Rab1 is generally known as a factor required for both ER-Golgi vesicular trafficking and Golgi maintenance, but it also has roles in ER tubulation and/or initiation of autophagy (23). Cells with the *Rab1* knockdown had GP64 surface levels that were reduced by approximately 50%. In those *Rab1* knockdowns, we observed increased perinuclear GP64 (Fig. 5), and detected large cytoplasmic GP64 puncta. The GP64-positive perinuclear ring colocalized with the lamin A-stained nuclear envelope. However, the GP64 puncta, which were mostly perinuclear, did not overlap either the lamin A or ER (calnexin 99A) stains. Large GP64 puncta colocalized with markers for Golgi, retromer, lysosomes, and late endosomes.

Rab4 localizes to sorting/recycling endosomes and is important for targeting proteins to the cell membrane. Both Rab4 and Rab11 are associated with sorting/recycling endosomes; Rab11 as part of the so-called "slow" route and Rab4 alternatively, as part of the "fast" route. The result from the knockdown of Rab11, although substantial, was not significant based on our selection criteria. On the other hand, the Rab4 knockdown was significant (Fig. 4C) and resulted in an approximately 50% reduction of surface GP64 levels (Fig. 4A). Dramatic accumulation of perinuclear GP64 (which overlapped with lamin A staining) was also observed in cells with a Rab4 knockdown. We observed large GP64-positive puncta that were localized both centrally and peripherally in cells, but they did not overlap with the ER marker. In the Rab4 knockdown cells, GP64 appeared to colocalize with Golgi and recycling endosomes (Fig. 5). Thus, GP64 accumulation in recycling endosomes in the Rab4 knockdown suggests that GP64 may be transported to the cell surface via sorting/recycling endosomes containing Rab4. Alternatively, GP64 may be transported more directly to the plasma membrane, then endocytosed and recycled to the cell surface. Further experiments are needed to understand GP64 accumulation in Rab4-depleted cells.

Snap29 was also identified as important for GP64 cell surface localization (Fig. 4). Snap29 is a multifunctional protein, with roles related to autophagy as well as endocytic and exocytic trafficking of proteins (24). The *Snap29* knockdown resulted in an approximately 50% reduction in surface GP64 levels in the screen. In Snap29 depleted cells, GP64 accumulated dramatically in the perinuclear region and colocalized with lamin A. Notably, GP64 accumulated strongly in the Golgi compartment and was also associated with Retromer complexes (Fig. 5, Snap29). We also noted that GP64 accumulation in Golgi-stained structures appeared at substantially higher levels than in Golgi from control cells, or cells with most other gene knockdowns. Although reduced levels of surface localized GP64 due to *Snap29* knockdown was documented from the screen, microscopy revealed a strong GP64 signal at the cell periphery, and colocalization with the plasma membrane marker (concanavalin A). This may suggest that GP64 accumulates below or very near the plasma membrane in the presence of the *Snap29* knockdown.

Gene knockdowns that resulted in increased GP64 cell surface levels. The RNAi screen was initially designed to identify cellular proteins that are important for GP64 transport to the cell surface and thus to identify gene knockdowns that resulted in a reduction of GP64 levels at the cell surface. Surprisingly, we also identified several gene knockdowns that significantly increased GP64 surface levels. The results from 3 gene knockdowns (*Rab5*, *Rab7*, and *Exo84*) that led to substantial increases in GP64 surface levels are shown in Fig. 6A (left). In the presence of each of these knockdowns, *gp64* mRNA levels were similar to those of the control *lacZ* dsRNA-treated cells (Fig. 6A, center), suggesting increased efficiency of GP64 trafficking or retention at the plasma

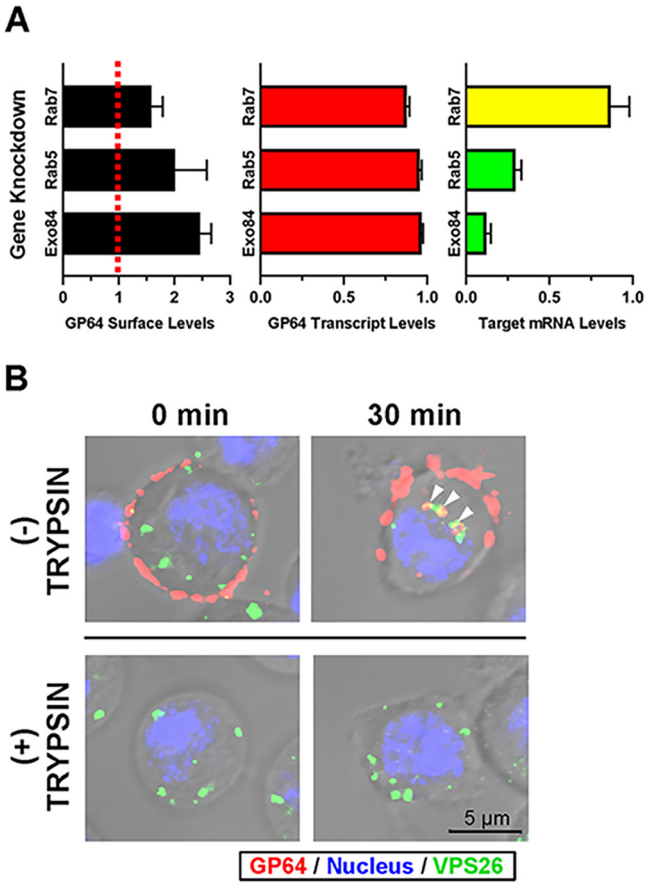

FIG 6 Validation and analysis of gene knockdowns that increased cell surface GP64 levels. (A) Identification and validation of several host genes for which dsRNA treatment resulted in increased cell surface GP64 levels. (Left) RNAi knockdowns of Rab7, Rab5, and Exo84 resulted in approximately 1.5- to 2.5-fold increases in GP64 cell surface levels (black bars) compared with control *lacZ* dsRNA, determined by flow cytometry as for Fig. 4 (the dashed red line indicates the relative control *lacZ* value). (Middle) *gp64* mRNA levels (red bars) in the presence of each of the RNAi knockdowns were determined by RT-qPCR and were similar to that from control cells treated with *lacZ* dsRNA (1.0 indicates control RNAi against *lacZ*). (Right) mRNAs from RNAi knockdowns of target host genes (*Rab5*, *Rab7*, and *Exo84*) were measured by RT-qPCR and compared with levels of the same mRNAs in the presence of a control *lacZ* dsRNA knockdown (1.0). *Rab5* and *Exo84*, but not *Rab7*, target mRNA levels were substantially depleted (>50%) after 4 days of treatment with the corresponding dsRNA. (B) Endocytosis of cell surface GP64. Cell surface GP64 was labeled with a GP64-specific monoclonal antibody (AcV1) by incubation at 4°C. As a control, trypsin was used to remove cell surface GP64 prior to GP64 immunolabeling [(+)Trypsin]. Cells were shifted to 27°C and allowed to endocytose GP64-Ab complexes for 30 min before fixation, permeabilization, and counterstaining with an anti-VPS26 antibody and analysis by confocal microscopy as described in Materials and Methods. GP64 (red) that was endocytosed was observed associated with VPS26 (retromer; green)-labeled organelles (arrowheads). Colocalization is indicated by yellow.

membrane. Cells treated with Exo84 or Rab5 dsRNA had highly efficient target mRNA depletion (12% and 29% of the control, respectively), whereas *Rab7* mRNA depletion was less efficient (86% of control) (Fig. 6A, right). However, it is notable that two independent Rab7-specific dsRNAs yielded the same approximate levels of increased cell surface GP64, suggesting that the phenotype is reproducible and results from depletion of Rab7. Rab5 functions in early endosomes, but it is also detectable at the plasma membrane (25), compatible with its known roles in CCV formation, fusion with early endosomes, and homotypic fusion between early endosomes (26, 27). Rab7 regulates transport from early to late endosomes and lysosomes, acting downstream of Rab5 (28, 29) in addition to playing an important role in autophagy (28, 30). Thus, Rab5 and Rab7 are both involved in postendocytic trafficking, whereas Exo84 is well established as a component of the exocyst complex that is required for targeting of vesicles to the

cell membrane for protein exocytosis and other events involving the plasma membrane (cytokinesis, cell growth, and ciliogenesis).

Cell surface GP64 is endocytosed. *Rab5* and *Rab7* knockdowns resulted in a 1.5× to 1.75× increase in cell surface GP64 compared with control cells, and considering that the major roles of Rab5 and Rab7 are in postendocytic trafficking, this suggested that GP64 may be continually endocytosed and transported through the endocytic pathway. To determine whether surface-localized GP64 is internalized into cells by endocytosis, we labeled cell surface GP64 with a GP64-specific antibody at 4°C (to inhibit endocytosis), then shifted the temperature to 27°C for 30 min, and assessed internalization of the GP64:Ab complexes after the inhibition of endocytosis was released. When cells were then fixed, permeabilized, and incubated with a secondary Alexa Fluor 555-conjugated anti-mouse antibody to detect GP64:Ab complexes, we detected intracellular GP64:Ab complexes. However, if cells were treated with trypsin to remove surface GP64 prior to binding of the primary anti-GP64 antibody, no internal GP64 was detected. The results demonstrated GP64 endocytosis from the cell surface. To gain insight into the potential fate of the endocytosed GP64, we also costained for a component of the retromer complex (VPS26). The major function of retromer is in retrieval of cargo proteins from the endolysosomal system back to the ER/Golgi compartment or sorting/recycling endosomes, for recycling back to the plasma membrane (31). We observed colocalization of the endocytosed GP64:Ab complexes with the marker for the retromer complex (VPS26) (Fig. 6B, green) suggesting that endocytosed GP64 may be recycled back to the plasma membrane, as is known to occur for viral envelope proteins from Nipah virus (32), respiratory syncytial virus (33), vesicular stomatitis virus (34), and varicella-zoster virus (35). We cannot eliminate the possibility that some of the GP64 endocytosed from the cell surface may also be trafficked through the endolysosomal system and eventually degraded. However, the observation that Rab5 and Rab7 depletion led to increased cell surface levels of GP64, and the fact that we observed endocytosis of GP64, together indicate that GP64 is not static at the cell surface once delivered there. Thus, at least a portion of the GP64 delivered to the cell surface appears to be endocytosed and is likely recycled back to the cell surface.

DISCUSSION

To examine the requirements for trafficking of the viral GP64 envelope protein in insect cells, we generated a cell line that inducibly expresses GP64 and used it to measure the effects of a variety of RNAi knockdowns on trafficking of GP64 to the plasma membrane. We selected *D. melanogaster* cells as an experimental system because of the plethora of genetic and molecular tools available for this system and *in vivo* tools and models available for extended future studies. We first developed an inducible cell line for expression of the GP64 protein and demonstrated that induction of GP64 expression was tightly regulated and robustly activated upon incubation of cells in Cu_2SO_4. Following GP64 induction, most of the GP64 was displayed on the cell surface, and only a small fraction of GP64 was found within the cell or released from cells in exosomes. Using the engineered cell line, we developed and performed an RNAi screen that targeted 213 cellular genes that included 13 groups of genes involved in vesicular trafficking. We identified 37 gene knockdowns that reduced GP64 surface levels by 40 to 90% and thus initially appeared to affect trafficking. To eliminate hits that may have resulted from indirect or pleiotropic effects on the cell (and not on GP64 trafficking), we selected hits with ≥50% of the control *gp64* mRNA levels and found that 13 of the original 37 hits met this criterion. The 13 hits included genes that encode Rab GTPases (and Rab effectors), clathrin and associated adaptors, and a SNAP protein. Among the 13 hits, we further assessed and confirmed the target gene knockdowns, and we selected 6 genes for further analysis. We then examined the cellular effects on GP64 trafficking from knockdowns of Rab GTPases (*Rab1* and *Rab4*), clathrin and associated adaptors (*Chc*, *AP-2μ*, and *AP-1-2β*), and *Snap29*.

Rab GTPases are regulators of vesicular trafficking that control vesicular interactions

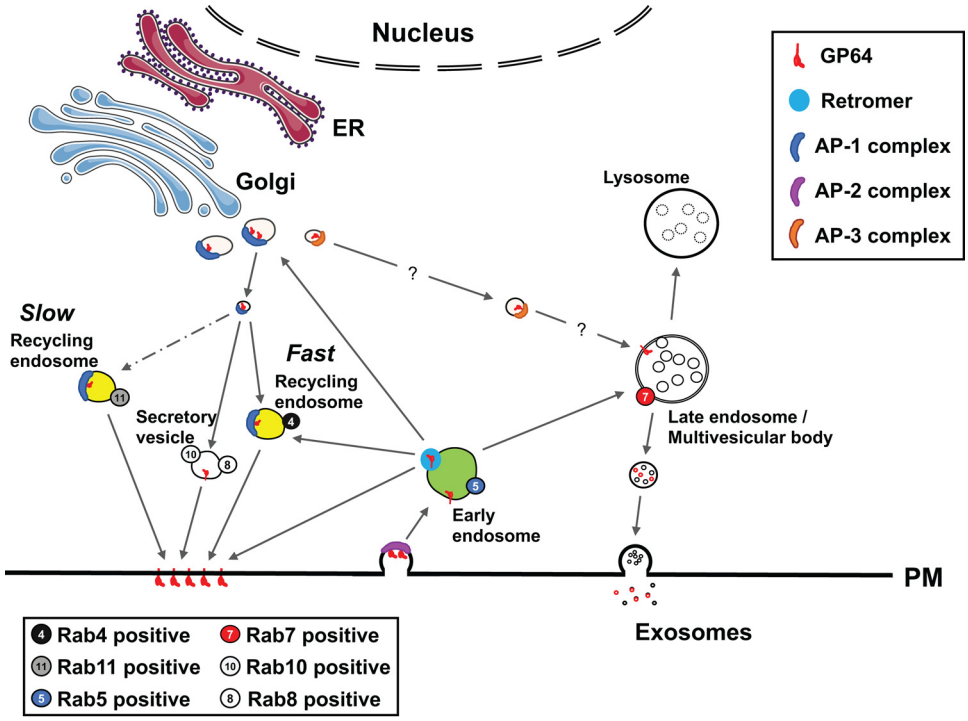

FIG 7 Model of GP64 trafficking in insect cells. The roles of cellular pathways, protein complexes, and individual proteins are illustrated based on known functions and localization patterns and from experimental data. Trimeric GP64 is synthesized, folded, and posttranslationally modified in the ER and Golgi compartment. The AP-1/clathrin complex mediates transport of selected membrane proteins from the Golgi compartment to the PM either directly in Rab8/Rab10-positive Golgi-derived secretory vesicles or indirectly through Rab4-containing (fast) or Rab11-containing (slow) recycling endosomes. Individual depletion of Rab4 or Rab11 reduced PM levels of GP64, although the effect of the Rab11 depletion (dashed line) was only moderate. The AP-2/clathrin complex is involved in clathrin-mediated endocytosis of PM-localized proteins. GP64 displayed on the PM was subsequently endocytosed and localized to retromer-containing endosomes, suggesting recycling of endocytosed GP64 to the PM. Recycling to the PM may occur either directly, or via the Golgi or recycling endosomes. AP-1-2β depletion resulted in a dramatic decrease in GP64 levels on the PM. In *Drosophila*, both the AP-1 and AP-2 adaptor complexes contain AP-1-2β. Thus, it is unclear whether lack of either AP-1 or AP-2 complex function (or both) is the cause of reduced GP64 PM levels. Depletion of either Exo84, Rab5, or Rab7 resulted in increased levels of GP64 at the PM, which may have resulted from disruptions in GP64 endocytosis or exocytosis.

and tethering of vesicles to discrete organellular membranes. Rab1 serves a variety of roles or functions, and is largely associated with the ER, Golgi compartment, and intermediate compartments (ERGIC) whereas Rab4 is localized to post-Golgi sorting/recycling endosomes (36, 37). The individual knockdown of *Rab1* or *Rab4* disrupted transport of GP64 to the cell surface, indicating that GP64 trafficking requires Rab1-assisted ER-to-Golgi trafficking, as well as Rab4-mediated post-Golgi sorting (Fig. 7). GP64 glycosylation in the Golgi compartment is necessary for proper folding and trimerization of the envelope fusion protein. It is understandable then that disrupted Rab1-mediated ER-Golgi transport should result in reduced GP64 transport within post-Golgi organelles, and accordingly, we saw that increased ER/Golgi GP64 accumulation reflected the reduced amount of cell surface GP64 with Rab1 depletion. The observation that Rab4 depletion also reduced GP64 trafficking to the cell surface suggests a necessary post-Golgi GP64 quality control or sorting step in Rab4-positive endosomes. Some proteins are transported directly from the Golgi to the PM, while others may traffic through sorting or recycling endosomes, and some proteins may use both routes to the PM (38). Proteins can be transported directly from the Golgi to the PM in a Rab8/Rab10-dependent manner. Otherwise, proteins may transit via either Rab11-positive or Rab4-positive endosomes and/or vesicles en route to the PM. In addition, proteins delivered to the cell surface may be subsequently endocytosed and then

trafficked through either Rab11-positive (slow) or Rab4-positive (fast) endosomes back to the cell surface. Because we found that cell surface GP64 is endocytosed and that the endocytosed GP64 associates with retromer, a molecular hub for recycling of endocytosed membrane proteins, this suggests that GP64 that is endocytosed might then be recycled back to the cell surface. Thus, it is unclear whether the requirement for Rab4 is for initial trafficking to the cell surface (via Rab4-positive sorting endosomes) or for maintenance at the cell surface via efficient recycling from the cell surface and back via Rab4 recycling endosomes. It is also possible that both are true, with Rab4 recycling endosomes involved in both the initial trafficking of GP64 to the cell surface and subsequently endocytosis and recycling back to the cell surface. It is also notable that a knockdown of Rab11 (another Rab GTPase known to localize to and function in slow recycling endosomes) also reduced GP64 surface levels, but the reduction was less severe (≤30% reduction) (Table S2). More detailed studies should better define the role of endosomes in the route(s) of GP64 transport and possibly recycling.

The knockdown of *Clathrin heavy chain* (*Chc*) and the *AP-2*μ and *AP-1-2*β clathrin adaptors comprised 3 of the 6 genes validated as important for GP64 transport. It is also notable that of these 6 selected genes, *Chc* and *AP-1-2*β represented the most severe reductions of GP64 plasma membrane levels (Fig. 4A). Formation of clathrin-coated vesicles (CCVs) occurs at many potential organellular membranes, but certain clathrin/AP complexes (5 known, 3 well described) are known to assemble at distinct membranes and have defined roles in directional subcellular transport: AP-1 CCVs assemble at the trans-Golgi network and traffic to recycling endosomes or the PM; AP-2 CCVs form at the PM and traffic to early, recycling, or sorting endosomes; and AP-3 CCVs form from Golgi membranes and transit toward late endosomes (39). AP complexes are heterotetrameric, each being composed of two large (one of $\gamma/\alpha/\delta/\varepsilon/\zeta$ and β1-5), a medium (μ), and a small (α) subunit. In mammals, there are also multiple isoforms of some subunits, but a single gene for each subunit exists in *D. melanogaster* and other invertebrates. In *Drosophila*, the AP-1 and AP-2 complexes share the AP-1-2β subunit (40), which was identified and validated as an important gene in our screen. Because AP-1-2β has functional roles in both AP complex 1 (secretory) and AP complex 2 (endocytosis), it is difficult to discern at which step GP64 transport is affected when AP-1-2β is depleted. RNAi of other members of the AP-1 or AP-2 complexes in our screen also did not elucidate further the requirement of either complex for GP64 trafficking. (Knockdowns of AP-1μ or AP-1σ had only modest effects, and knockdowns of AP-2α or AP-2σ had modest or inconsistent effects, respectively, on GP64 surface levels. See Table S2.) It is also noted that we found that surface localized GP64 was endocytosed and routed to retromer-labeled endosomes, implying that GP64 was recycled back to the PM. Thus, while the precise role(s) of the AP-1-2β subunit is not clearly distinguished, overall it appears that both AP-1 and AP-2 CCVs contribute to GP64 trafficking, with roles in post-Golgi compartment anterograde trafficking and retrograde recycling from the PM, respectively.

The specificity of the AP complexes 1 to 3 to transport cargo proteins lies in the amino acid motifs present on the cytoplasmic domains of cargo proteins they bind. AP complex binding to cargo protein motifs is attributed to either the μ subunit, which binds tyrosine-based YXXØ (where Y is tyrosine, X is any amino acid, and Ø is an amino acid with a bulky hydrophobic group) motifs, or the combination of the γ-σ1, α-σ2, and δ-σ3 subunits (of AP complexes 1 to 3, respectively), which bind dileucine-based (DE)XXXL(LI) motifs. GP64 has a YXXØ motif in its cytoplasmic tail but no sequence that resembles the dileucine motif. YXXØ motifs are bound by the μ1, μ2, and μ3 subunits (of the AP-1, AP-2, and AP-3 complexes, respectively) (39, 41). A YXXØ motif in a cargo protein, when bound by μ1 of an AP-1 complex in the Golgi and post-Golgi vesicles, typically promotes its transport to the PM, although additional motifs may modify the precise trafficking pathway. The mammalian AP-1 μ1A is required for basolateral transport of YXXØ-containing membrane proteins. The *Drosophila* AP-1μ ortholog, although much less well characterized, is also implicated in basolateral protein

trafficking, since Sanpodo (an AP-1-dependent cargo protein trafficked to basolateral membranes) accumulates apically in *Drosophila* sensory organ precursor cells with depleted/mutant AP-1μ (42). This suggests that *Drosophila* AP-1μ, like its mammalian ortholog AP-1 μ1A, is responsible for basolateral transport of YXXØ-containing cargo. In our screen, we detected only modest reductions (<20%) in GP64 surface levels for three independent dsRNAs targeting *AP-1μ*, but we did not confirm GP64 mRNA levels or *AP-1μ* knockdown efficiency in cells exposed to those dsRNAs. YXXØ motifs on cell surface membrane proteins, through interaction with μ2 of AP-2 complexes, promote internalization of the YXXØ-harboring proteins via clathrin-dependent endocytosis. Although it has yet to be functionally characterized in detail, the GP64 YXXØ motif is a likely candidate for directing the initial PM targeting of GP64 and also its subsequent internalization by endocytosis, as observed in DL1:mtGP64 cells. In prior studies in which the TM and cytoplasmic domains of AcMNPV GP64 were deleted or substituted with sequences that do not contain a YXXØ motif, the cell surface localization of GP64 was dramatically reduced (43, 44), suggesting that this motif plays a role in the initial targeting of GP64 to the PM or its maintenance there. Currently, the fate of endocytosed GP64 is unclear. Postendocytic trafficking could lead to lysosomal degradation, or the endocytosed GP64 may be recycled to the cell surface or released from cells by exocytosis, as we observed (Fig. 1C and D).

We demonstrated endocytosis of cell surface GP64 and its subsequent association with retromer, suggesting that GP64 may be recycled to the cell surface. However, if the endocytosed GP64 is not returned to sorting/recycling endosomes or the Golgi compartment, it could follow the endocytic route to late endosomes/multivesicular bodies and be released from cells in exosomes. We confirmed that DL1:mtGP64 cells produce exosomes containing GP64, albeit at very low levels in the context of our assay kinetics (8-h induction period). The μ3 subunit of AP-3 complexes also binds YXXØ motifs and directs transport of YXXØ-containing cargo proteins from the Golgi compartment to late endosomes/multivesicular bodies. We cannot determine from our current data whether AP-3-mediated trafficking of GP64 to late endosomes/multivesicular bodies occurs. Furthermore, we do not know what proportion, if any, of the endocytosed GP64 is recycled to sorting/recycling endosomes or the Golgi. Therefore, further studies will be required to determine which pool(s) of GP64 in cells is affected by knockdown of *Chc*, *AP-2μ*, *AP-1-2β*, or *Rab4*.

Although the RNAi screen was developed to identify gene knockdowns that reduce GP64 transport to the PM, we also detected significantly increased (0.5- to 2.5-fold) GP64 cell surface levels that resulted from several gene knockdowns. The most dramatic GP64 increases were observed from knockdowns of *Exo84* (2.5-fold), *Rab5* (1.75-fold), and Rab7 (0.5-fold). We confirmed normal *gp64* mRNA levels in cells with each of these knockdowns and a robust depletion (<20%) of *Exo84* and *Rab5* mRNAs, as well as a minor depletion of *Rab7* (86%). We did, however, note that two independent Rab7 dsRNA knockdowns yielded similarly increased GP64 surface levels. Rab5 and Rab7 localize to and have roles in sequential postendocytic trafficking organelles (early endosome [EE], late endosome [LE], multivesicular body [MVB], and lysosome [LYS]), so the observed increase of surface GP64 levels from these knockdowns could result from trafficking defects in the same trafficking pathway.

When cell surface proteins (i.e., GP64) are endocytosed, the internalized endocytic vesicles that are pinched off have Rab5 on their cytosolic surface. Endocytic vesicles containing Rab5 fuse with EEs, a process that begins with Rab5 interacting with early endosome antigen 1 (EEA1) of EEs. Rab5-positive endosomes containing the cargo protein (GP64) transition to Rab7-positive LEs in a manner involving a coregulated Rab5-Rab7 exchange. For this, Rab5 stimulates endosome acquisition of Rab7 by recruiting the Rab7 GTPase exchange factor (GEF; the Mon1/Ccz complex), and Rab7 in turn brings in the GTPase-activating proteins (GAP) for Rab5 (45). Because we found that GP64 was endocytosed from the cell surface, it is possible that the Rab5 and Rab7 knockdowns resulted in a reduction in endocytosis and thus an accumulation of GP64 at the surface.

There also exists the possibility that bifurcated trafficking of the endocytosed GP64 within in Rab5-positive endosomes occurs (Fig. 7). Rabaptin-5 (a Rab effector) binds both Rab5 and Rab4, via distinct binding sites, promoting cargo (GP64) transfer from early endosomes to Rab4-positive recycling endosomes (46). At least a minor portion of the GP64 is trafficked to LEs/MVBs, because GP64 is present in exosomes presumably derived from MVBs (Fig. 1 and 7). However, we do not know the original source of GP64 present in exosomes, since GP64 may be transported to LEs/MVBs by either (i) the PM endocytosis-Rab5-Rab7 pathway or (ii) the AP-3 complex, which assists sorting and transport of YXXØ-containing cargo proteins (such as GP64) from the Golgi to LEs/MVBs. It should be noted that in our screen we also observed reductions in GP64 surface levels for knockdowns of two of the three AP-3 components (cm and rb). For the YXXØ-binding μ3 ortholog (cm) and the β3 ortholog (rb) we saw moderate to substantial reductions (Fig. 4A; Table S2) but only for a single gene-specific dsRNA. Further studies will be required to understand the precise roles of Rab5 and Rab7 and the pathways involved in GP64 trafficking.

Sorting/recycling endosomes are also known to sometimes play important roles in basolateral trafficking in polarized epithelia. Proteins targeted to basolateral membranes can either traffic directly from the TGN (47) or traffic first through sorting/recycling endosomes before surface delivery (38) (Fig. 7). During the primary phase of the infection, GP64 traffics to basal membranes of polarized lepidopteran midgut epithelial cells, facilitating basolateral release of infectious budded viral progeny into the hemocoel (2). In the subsequent systemic infection, many cell types are infected, and those cells may have divergent states of polarity and thus trafficking pathways. It is possible that GP64 may be transported via several trafficking pathways as a means of efficient virus assembly and budding from different cell types that are infected in the animal. In the current study, we used the power of a relatively broad screen in *Drosophila* cells to identify host proteins and to provide clues to the specific pathways utilized for trafficking of this important viral envelope protein. In addition to further studies to refine the results of the current study, it will also be important in future studies to examine determinants of polarized GP64 protein transport in cells of critical tissues, such as the midgut epithelium, and in an insect model. Understanding viral trafficking in tissues that are critical for successful infection will have relevance not only to insect-pathogenic viruses, such as baculoviruses, but also to arboviruses and plant viruses that are transmitted by insects and that must also navigate cells of the polarized midgut epithelium. We are continuing these studies in a *Drosophila*-based *in vivo* model system.

MATERIALS AND METHODS

Cell line generation and analysis. (i) Plasmids. To generate a *Drosophila* cell line for inducible expression of the baculovirus GP64 protein, the AcMNPV *gp64* gene coding region (NCBI NC_00162) was cloned under the transcriptional control of a *metallothionein* promoter and inserted into the genome of *Drosophila* DL1 cells (https://dgrc.bio.indiana.edu/product/View?product=9), as described below. The AcMNPV *gp64* open reading frame (ORF) was subcloned into the EcoRI site of vector pMT-V5-His (Invitrogen) to generate plasmid pMT-GP64 (in which *gp64* is out of frame with the *V5* and *6× His* codons).

(ii) Cells. Adherent *Drosophila* DL1 cells and DL1-derived cell lines were grown in Schneider's medium (Gibco, catalog no. 21720024) supplemented with 8% fetal bovine serum (FBS) (HyClone).

(iii) Transfection and selection of a stable cell line. *Drosophila* DL1 cells (5.0×10^5 cells in a 35-mm well) were cotransfected (48) with 2 μg of a plasmid mixture containing a 5:1 mass ratio of pMT-GP64:pCoPuro (Addgene no. 17533) and incubated for 72 h in the absence of antibiotic. Transfected cells were then selected in growth medium containing 400 μg/mL puromycin (Invitrogen) over 10 days, with subculturing every 3 days into fresh medium containing 400 μg/mL puromycin. The puromycin-selected cells were then induced to express GP64 by incubation in medium containing 500 μM Cu_2SO_4 for 12 h. Cell surface GP64 was detected by flow cytometry analysis of live cells using the GP64-specific primary antibody AcV1 (49) and an Alexa Fluor 555-conjugated donkey anti-mouse secondary antibody (Invitrogen). Approximately 50% of the induced cells displayed GP64 at the cell surface. GP64-positive cells were then isolated (1 cell/well in a 96-well plate) with a BD Biosciences FACSAria Fusion fluorescence-activated cell sorter (FACS), and a single-cell clone was named DL1:mtGP64. After 8 passages of the clonal DL1:mtGP64 cells, GP64 expression was induced (50 μM Cu_2SO_4, 8 h) and GP64 was detected on the surface of 99% of the cells by flow cytometry, using a phycoerythrin-conjugated AcV1 antibody (Thermo Fisher, catalog no. 12-6991-82). The DL1:mtGP64 clonal cell line was then expanded, frozen in

aliquots, and stored in liquid nitrogen. For continuing studies, DL1:mtGP64 cells were grown at 22°C and used for approximately 50 passages before a new aliquot was resurrected.

Gene-specific dsRNA selection and production. For RNAi knockdowns of genes potentially involved in trafficking of the GP64 protein, gene-specific dsRNAs were identified and selected from the *Drosophila* RNAi Screening Center (DRSC) database (Harvard Medical School) (50). We selected 213 genes belonging to 13 gene groups (Table 1) and for each, we selected target gene sequences (100 to 1,300 nucleotides [nt]) that lacked potential off-target effects. Up to three independent dsRNAs specific for each selected gene were identified for the assay, and the resulting 561 target sequences are listed in Table S1, with the DNA primers used for amplifying the target sequences. dsRNAs for RNAi were transcribed from dsDNA templates with T7 RNA polymerase, purified on Qiagen RNeasy columns, adjusted to 50 ng/μL in nuclease-free water (GrowCells, catalog no. NUPW-1000), and arrayed (750 ng in 15 μL per well) into sterile 96-well tissue culture plates (BioOne) by the DRSC (https://fgr.hms.harvard.edu/). dsRNAs in assay plates were stored sealed at −60°C. For RNAi knockdown experiments, each assay plate contained 60 wells with dsRNAs, which included 54 individual gene-specific dsRNAs, three wells with the negative-control *lacZ* dsRNA, and three wells with the positive-control Rab1 dsRNA (Table S1).

dsRNA treatment of cells. To initiate RNAi knockdowns in DL1:mtGP64 cells, cells were incubated in culture medium containing a gene-specific or control dsRNA according to the protocol described by the DRSC (50). Briefly, DL1:mtGP64 cells grown to near confluence were resuspended in serum-free Schneider's medium at 1.67×10^6 cells/mL. Cells (50,000 in 30 μL medium) were added to each well of the assay plates which already contained dsRNA (15 μL/well; 50 ng/μL). Plates were incubated at room temperature for 30 min before addition of 55 μL of Schneider's medium containing 16% FBS to each well. Plates were then incubated at 22°C for 4 days before induction of GP64 expression. To induce GP64 expression, 50 μL of Schneider's medium (containing 8% FBS and 300 μM Cu_2SO_4) was added to the growth medium in each well by gentle iterative (5×) pipetting with a multichannel pipette for a final concentration of 100 μM Cu_2SO_4.

Optimization of the RNAi assay. To optimize the RNAi knockdown assay, we assessed the effects of Cu_2SO_4 concentration and incubation time on GP64 cell surface levels in dsRNA-treated DL1:mtGP64 cells. Cells were first incubated in 750 ng (7.5 ng/μL) of either *lacZ* (negative control) or Rab1 (positive control) dsRNA at 22°C for 4 days, as described above. Then, the growth medium was replaced with 100 μL of Schneider's medium (with 8% FBS) containing various Cu_2SO_4 concentrations (2-fold dilutions of Cu_2SO_4 from 12.5 to 400 μM) in each well of the dsRNA-treated cells. After an incubation of 8 h, relative cell surface levels of GP64 were measured by flow cytometry. After the Cu^{2+} induction period, plates were placed on ice for 30 min, then monolayers of cells were washed twice with 200 μL of ice-cold phosphate-buffered saline (PBS) (pH 7.5) and then incubated with 50 μL of ice-cold blocking solution (3% bovine serum albumin [BSA], 1% normal donkey serum [NDS] in PBS, pH 7.5) for 30 min. Blocking solution was then replaced with 50 μL of a solution containing a phycoerythrin-conjugated anti-GP64 monoclonal antibody (AcV1, Invitrogen; 1/250 dilution) in 1% BSA and 1% NDS, and incubated on ice in the dark for 2 h. The antibody solution was removed and cells were washed three times with 100 μL cold PBS (pH 7.5) before resuspension in 100 μL cold PBS with a p200 pipettor. Cells were analyzed for relative GP64 cell surface levels by flow cytometry on an Accuri C6 flow cytometer, using the FLA 2 (585/40) filter. The geometric mean of fluorescence in each well was determined for the entire population of cells. Relative GP64 levels were compared among *lacZ* dsRNA-treated cells induced with various Cu_2SO_4 concentrations for 8 h to determine effects of Cu_2SO_4 dose on GP64 surface levels. We also compared relative GP64 levels among control *lacZ* and Rab1 dsRNA-treated cells to determine effects of various Cu_2SO_4 doses and incubation times on the effects of the Rab1 knockdown. Overall, we determined that induction of GP64 expression with 50 to 200 μM Cu_2SO_4 for 8 h provided the most sensitive conditions for analysis of the effects of RNAi knockdowns. A Z-factor was also calculated to assess the feasibility of this 8-h induction scheme to identify genes that, when knocked down, cause reduced transport of GP64 to the cell surface. The total mean cellular fluorescence values of the (negative) *lacZ* and (positive) Rab1 dsRNA-treated cell controls were used to calculate a Z-factor of 0.67 for this assay. A Z-factor from 0.5 to 1.0 defines an assay that should be capable of identifying hits in an RNAi-based screen (15).

Targeted RNAi screen. To examine the effects of 213 host gene knockdowns on GP64 transport to the cell surface, we analyzed DL1:mtGP64 cells incubated individually with 561 dsRNAs representing multiple target sites for each of the 213 genes. Each 96-well assay plate contained 54 unique dsRNAs targeting host genes, plus 3 positive- and 3 negative-control wells. Three plates were prepared and assayed simultaneously, and replicates of the 3 plates were prepared and assayed on each of three separate days (3 biological replicates). Following an 8-h induction of GP64 expression, the geometric mean fluorescence measurement of GP64 detected at the cell surface was calculated for each of the dsRNA-treated cell samples using FCS Express software. The value from each gene-specific dsRNA was assessed on a plate-by-plate basis, by comparison to either (i) the geometric mean of values from all wells from the same plate or (ii) the geometric mean of the *lacZ* negative controls on the same plate (Table S2). To identify hits in the two data sets, analysis of variance (ANOVA) was used for comparisons using either the plate average or the *lacZ* average, and dsRNA knockdowns that resulted in a ≥40% reduction of GP64 surface levels, with a P value of ≤0.05 in both calculations, were scored as hits (Table S2). Genes identified by this means as having a potential role in GP64 transport to the cell surface are listed in Table S3.

RT-qPCR of *gp64* and *Drosophila* gene transcripts. To identify gene hits that resulted from effects on GP64 transport to the plasma membrane, and to eliminate hits resulting from pleiotropic effects on *gp64* transcription, the *gp64* mRNA levels of the 37 potential hits were analyzed by reverse transcription-quantitative PCR (RT-qPCR). DL1:mtGP64 cells were first incubated with dsRNAs specific for each of the

37 potential hits (or the *lacZ* control) as described above for the initial screen. *gp64* gene expression was then induced by incubation in 100 μM Cu_2SO_4 for 8 h, and total RNA was then isolated from each of three wells of cells in a 96-well plate, using TRIzol according to the manufacturer's protocol. Total RNA was resuspended in water and quantified using a Nanodrop spectrophotometer. Each RNA sample (100 ng) was used for reverse transcription with a QScript cDNA synthesis kit (Quantabio) that uses both oligo$(dT)_{18}$ and random hexamers for reverse transcription. cDNAs were diluted 1:100 in nuclease-free water, and 1 μL was used for PCR amplification of *gp64* or *Drosophila rp49*. The *gp64* primers were 5′-GGCAACACGACCTATCACGA-3′ (forward) and 5′-ATTCGCCTTCAGCCATGGAA-3′ (reverse). The *rp49* primers used were 5′-GACGCTTCAAGGGACAGTATCTG-3′ (forward) and 5′-AAACGCGGTTCTGCATGAG-3′ (reverse). The mean relative *gp64* transcript levels for each of the potential hits and controls were quantified (using the cycle threshold [$\Delta\Delta C_T$] method) from the three independent dsRNA-treated cellular RNA samples.

Knockdown efficiency of selected hits. To verify knockdowns of selected target *Drosophila* gene hits, the procedure for RT-qPCR described above was followed, but with primers directed at each of the selected target genes: *Rab1* (5′-GTATACGATTGCACGGACCAGG-3′ and 5′-AAGTCGCTCTTGTTGCCAACC-3′), *Rab4* (5′-TTGAAGAGGCCTTTCTCAAGTGC-3′ and 5′-AGCTCCGCCGTACTGAATACC-3′), *AP-1-2*β (5′-ACGTGTCCGCCCTCTTCC-3′ and 5′TCGCAGTCCTTCACGAACG-3′), *AP-2*μ (5′-GGCGGCTGTGACCAAGC-3′ and 5′-GCCGAAGTAGGATTGCATCACC-3′), *Chc* (5′-AAGGCTGTCGATGTCTTCTTTCCG-3′ and 5′-TATATGCACGTGGCCGTCTCC-3′), *GAPsec* (5′-CCTGCAAGATCATCCGCTGAG-3′ and 5′-AATCGGTGGGCTGCTGG-3′), CG16896 (5′-CTCAATTCTTGGGGTCGACGG-3′ and 5′-GCTGCCGAAACGCATCAGAG-3′), and *Snap29* (5′-GCAGAACAAACGGACGGGAG-3′ and 5′-TTCTCAGCATAGGCCAGTCG-3′). The mean relative transcript levels for each of the target gene hits were quantified ($\Delta\Delta C_T$) and normalized to that quantified ($\Delta\Delta C_T$) for the corresponding transcript from *lacZ* dsRNA-treated cells.

Immunolocalization of GP64 and organelles in dsRNA-treated cells. To examine GP64 localization in the presence of selected gene knockdowns, GP64 immunolocalization was performed in cells following dsRNA-mediated knockdowns and induction of GP64 expression. Briefly, DL1:mtGP64 cells were incubated with the selected dsRNAs in a well of a 96-well plate as described above. After 4 days of incubation, cells were resuspended in PBS (pH 7.5, room temperature) and seeded onto zones (limited with a liquid-blocking PAP pen) on sterile, poly-L-lysine-coated coverslips in 6-well plates (6 for each gene knockdown). GP64 expression was induced by the addition of Cu_2SO_4 (200 μM) for 16 h at 22°C. Alexa Fluor 647-conjugated concanavalin A (Thermo Fisher, C21421) was used to identify cell boundaries. Cells were incubated with the concanavalin A-Alexa Fluor 647 (100 μg/mL in PBS, pH 7.5) on ice for 30 min in the dark, then rinsed three times with cold PBS (pH 7.5), and fixed in the dark with paraformaldehyde (4% in PBS, pH 7.5) at 4°C for 30 min. The fixative was removed and coverslips were rinsed three times (5 min/rinse) with PBS (pH 7.5) at room temperature. Cells were permeabilized by incubating in 0.1% Triton X-100 (in PBS, pH 7.5) for 10 min at room temperature and then incubated in blocking solution (3% BSA, 1% NDS, 0.1% Triton X-100 in PBS, pH 7.5) for 30 min at room temperature. Cells were incubated with primary antibodies overnight (16 h) at 4°C in the dark. GP64 and organelles were stained with specific antibodies (see below) in antibody staining solution (1% BSA, 1% NDS, 0.1% Triton X-100 in PBS, pH 7.5). The primary antibody solution was removed, and cells were rinsed with PBS (three times for 10 min at room temperature); cells were then incubated with a secondary Alexa dye-conjugated antibody (each diluted 1:1,000 in antibody staining solution) for 4 h at room temperature in the dark. Nuclei were stained by addition of DAPI (4′,6-diamidino-2-phenylindole; 5 mM in PBS, pH 7.5) for 30 min; then, excess DAPI and secondary antibodies were removed and cells washed three times for 10 min with PBS (pH 7.5) before coverslips were mounted in a glycerol-based antifade buffer (CitiFluor). Cells were photographed using a SP2 Zeiss confocal microscope (750 TLM) using a 63× oil immersion lens and a 2.5× digital zoom.

Analysis of extracellular vesicles. For isolation of extracellular vesicles (EVs), DL1 or DL1:mtGP64 cells (2.5×10^7) were plated in 100-mm culture dishes in Schneider's growth medium with 8% FBS. Cell monolayers were washed three times with 10 mL room temperature PBS (pH 7.5); then, growth medium containing 200 μM Cu_2SO_4 was added to induce GP64 expression. Uninduced DL1:mtGP64 cells were similarly washed but were incubated in fresh Schneider's medium without Cu_2SO_4. Cells were then incubated for 8, 16, or 24 h, followed by separate collection of cells and supernatant. For control DL1:mtGP64 cells lacking Cu_2SO_4 treatment and for control DL1 cells exposed to Cu_2SO_4-containing medium, cells and corresponding supernatants were collected separately after 24 h.

EVs were isolated from the cell culture medium by the following procedure. The medium was first centrifuged at 3,000 × *g* for 10 min at room temperature to pellet floating cells or large debris. The supernatant was then collected and centrifuged at 10,000 × *g* for 30 min at 4°C to pellet additional cellular debris. The clarified medium (approximately 11 mL) was then underlaid with 1 mL 25% sucrose, and EVs were pelleted at 100,000 × *g* for 2h at 4°C in a Beckman Optima XE-90 ultracentrifuge using an SW-41 rotor (12.5-mL tubes). The resulting EV pellet was resuspended in 12 mL PBS (pH 7.5) and then repelleted (100,000 × *g*, 2 h, 4°C). The EV pellet was subsequently resuspended in 50 μL PBS (pH 7.5) and stored at −20°C until analysis by immunoblotting. Eleven milliliters of the Cu_2SO_4-containing Schneider's growth medium was used as a control for possible EVs derived from the FBS supplement. For analysis of cell lysates, the cells from each 100-mm plate were resuspended in PBS (pH 7.5), then pelleted by centrifugation (1,000 × *g*, 10 min, room temperature), and lysed in 200 μL of lysis buffer (1% Triton X-100, 100 mM NaCl, 10 mM Tris; pH 7.5) supplemented with a protease inhibitor cocktail (Roche cOmplete, EDTA-free protease inhibitor cocktail). EV preparations or cell lysate samples were mixed with an equal volume of 2× SDS-PAGE loading buffer and heated to 95°C for 10 min; then, proteins were resolved on a SDS–12% polyacrylamide gel. For comparisons of relative levels, cell lysate

samples were serially diluted 2-fold in 1× SDS-PAGE loading buffer. For immunoblotting, 5% of each total EV pellet and 0.5% of each total cell lysate was loaded onto each lane of an SDS-PAGE gel.

Sucrose gradient fractionation of EVs. To identify EVs from the supernatants of GP64-expressing DL1:mtGP64 cells, 12 178-mm culture plates were seeded with approximately 1×10^7 DL1:mtGP64 cells, and cells were grown to approximately 70% confluence (3 to 4 days). Cells were washed three times with PBS (pH 7.5, room temperature) and then incubated at 22°C in 17 mL/plate of Schneider's growth medium containing Cu_2SO_4 (200 μM). After a 24-h incubation period, EVs were purified from the culture medium by the protocol described above, but using 6 tubes (35 mL/tube) in a Beckman SW-32 rotor. The resulting six EV pellets were resuspended in a total of 600 μL PBS (pH 7.5) and applied to a 12-mL sucrose step gradient (3 mL 80%, 2.5 mL 60%, 2.5 mL 45%, 2.5 mL 30%, and 2 mL 15% sucrose) and centrifuged to equilibrium (100,000 × *g* for 18 h at 4°C). Twelve 1-mL fractions were collected from the top to bottom of the gradient. EVs were purified from 0.5 mL of each 1 mL fraction by mixing with 1 mL of PBS (pH 7.5) and pelleting at 100,000 × *g* for 2 h at 4°C, in capped conical 1.5-mL tubes (Beckman) using a TLA 55 rotor (Beckman Optima TLX ultracentrifuge). Each EV pellet was resuspended in 20 μL of 1× SDS-PAGE loading buffer, and 5 μL was loaded onto a 0.75-mm 12% polyacrylamide SDS-PAGE gel. The resolved proteins were then electroblotted onto polyvinylidene fluoride membranes for Western blot analysis.

GP64 endocytosis assay. To examine endocytosis of GP64 from the cell surface, DL1:mtGP64 cells (approximately 2×10^5) were seeded onto zones (limited with a liquid-blocking PAP pen) on sterile, poly-L-lysine-coated coverslips in 6-well plates. Growth medium (2.5 mL) containing Cu_2SO_4 (200 μM) was added to cells to induce GP64 expression, and cells were incubated at 22°C for 12 h. Plates were then placed on ice for 30 min, and coverslips were washed three times with 3 mL cold PBS (pH 7.5) to inhibit endocytosis. Control coverslips were then incubated with 2.5 mL ice-chilled 1× trypsin-EDTA (0.25%, Gibco catalog no. 25200056) on ice for 30 min, and washed three times with 3 mL cold PBS, while other coverslips were maintained on ice in PBS. Coverslips (trypsin treated and untreated) were incubated with an anti-GP64 antibody (AcV1; diluted 1:100 in cold PBS, pH 7.5) on ice for 2 h; then, the antibody solution was removed, and cells were washed three times with 3 mL cold PBS (pH 7.5). After washing, coverslips were either retained on ice to block endocytosis or transferred to growth medium in prewarmed (27°C) 6-well plates and incubated for 30 min to permit endocytosis of GP64-AcV1 antibody complexes. After incubation at 27°C for 30 min, cells on coverslips transferred to 27°C were fixed for 30 min in 2.5 mL of 4% paraformaldehyde in PBS at room temperature. Cells retained on ice were fixed with 2.5 mL cold 4% paraformaldehyde in PBS on ice for 30 min. Cells were permeabilized with Triton X-100 (0.1% in PBS) for 10 min at room temperature and then blocked with 3% BSA in PBS with 0.1% Triton X-100. Cells were then incubated with an anti-VPS26 antibody (a gift from Hugo Bellen) at 4°C overnight. After being washed three times with PBS, cells were incubated with a solution of Alexa Fluor 555-conjugated donkey anti-mouse antibody (for detection of AcV1-GP64 complexes) and Alexa Fluor 488-conjugated goat anti-guinea pig antibody (for detection of VPS26).

Immunoblotting. Protein samples were mixed with an equal volume of 2× SDS-PAGE loading buffer (4% SDS, 20% glycerol, 200 mM β-mercaptoethanol, 0.01% bromophenol blue, 0.1 M Tris HCl; pH 6.8) and denatured at 95°C for 10 min. For dilutions, denatured samples were diluted in 1× SDS-PAGE loading buffer. Proteins were resolved on 12% polyacrylamide SDS-PAGE gels and electroblotted to polyvinylidene fluoride membranes; then, blots were blocked in 5% skim milk in TBST (20 mM Tris, 150 mM NaCl, 0.05% Tween 20). Primary and secondary antibodies were diluted in 1% skim milk in TBST and incubated with blots at 4°C overnight or for 2 h at room temperature. Blots were washed three times for 10 min per wash with TBST. Signal from the horseradish peroxidase (HRP)-conjugated secondary antibodies was detected using SuperSignal West Pico Plus chemiluminescent substrate (Thermo Fisher) and a Bio-Rad ChemiDoc imaging system.

Antibodies. For flow cytometry and endocytosis assays, GP64 was detected with monoclonal antibody AcV1. AcV1 used for the RNAi screen was conjugated with phycoerythrin (Thermo Fisher, catalog no. 12-6991-82). For immunoblots, GP64 was detected with monoclonal antibody AcV5, and for confocal microscopy of fixed cells, GP64 was detected either with AcV5 or with a rabbit polyclonal anti-GP64 antibody (SinoBiological, 40496-RP01). Syntaxin 1A was detected on immunoblots with monoclonal antibody 8C3 (Developmental Studies Hybridoma Bank [DSHB] from S. Benzer and N. Colley). Organelles were identified in fixed cells using the following antibodies: goat polyclonal anti-golgin 245 and goat polyclonal GMAP (DSHB; S. Munro), used together to label the Golgi; mouse monoclonal anticalnexin 99A (DSHB; S. Munro; product Cnx99A 6-2-1) to label the endoplasmic reticulum; mouse monoclonal anti-Rab7 (DSHB; S. Munro; Hybridoma Product Rab7) to label early/late endosomes; rabbit polyclonal anti-cathepsin L/MEP antibody (Abcam, ab58991) to label lysosomes; mouse monoclonal antilamin DmO (DSHB; P. A. Fisher; hybridoma product ADL67.10) to label the nuclear envelope, mouse monoclonal anti-Rab11 (BD Biosciences, no. 610656) to label recycling endosomes; and guinea pig polyclonal anti-VPS26 (a gift from Hugo Bellen) to label the retromer complex.

SUPPLEMENTAL MATERIAL

Supplemental material is available online only.

SUPPLEMENTAL FILE 1, XLSX file, 0.3 MB.

ACKNOWLEDGMENTS

We thank Peter Nagy and Robin Chen for their comments on the manuscript and Stephanie Mohr of the Drosophila RNAi Screening Center at Harvard Medical School for assistance implementing bioinformatics, screen design, amplicon selection, dsRNA synthesis,

and arraying in assay plates. We also thank Sara Cherry for supplying the DL1 cells and Christopher Donahue (Cornell Veterinary Flow Cytometry) for assistance in isolating the clonal DL1:mtGP64 cell line. We thank the contributors to the Developmental Studies Hybridoma Bank at the University of Iowa for sharing antibodies: syntaxin 1A monoclonal antibody 8C3 (from S. Benzer and N. Colley); mouse monoclonal anticalnexin 99A, mouse monoclonal anti-Rab7, goat polyclonal anti-golgin 245m and goat polyclonal GMAP (from S. Munro); and mouse monoclonal antilamin DmO ADL67.10 (from P. A. Fisher). We are also grateful for the guinea pig polyclonal anti-VPS26 antibodies, a gift from Hugo Bellen.

This work was supported by NSF grants 1653021 and 2024252 to G.W.B. and N.B. and USDA grant 2021-67013-33569 to G.W.B.

REFERENCES

1. Robinson M, Schor S, Barouch-Bentov R, Einav S. 2018. Viral journeys on the intracellular highways. Cell Mol Life Sci 75:3693–3714. https://doi.org/10.1007/s00018-018-2882-0.
2. Blissard GW, Theilmann DA. 2018. Baculovirus entry and egress from insect cells. Annu Rev Virol 5:113–139. https://doi.org/10.1146/annurev-virology-092917-043356.
3. Ohkawa T, Welch MD. 2018. Baculovirus actin-based motility drives nuclear envelope disruption and nuclear egress. Curr Biol 28:2153–2159.E4. https://doi.org/10.1016/j.cub.2018.05.027.
4. Heigwer F, Port F, Boutros M. 2018. RNA interference (RNAi) screening in Drosophila. Genetics 208:853–874. https://doi.org/10.1534/genetics.117.300077.
5. Grabowska K, Wachalska M, Graul M, Rychlowski M, Bienkowska-Szewczyk K, Lipinska AD. 2020. Alphaherpesvirus gB homologs are targeted to extracellular vesicles, but they differentially affect MHC class II molecules. Viruses 12:429. https://doi.org/10.3390/v12040429.
6. Yang L, Li J, Li S, Dang W, Xin S, Long S, Zhang W, Cao P, Lu J. 2021. Extracellular vesicles regulated by viruses and antiviral strategies. Front Cell Dev Biol 9:722020. https://doi.org/10.3389/fcell.2021.722020.
7. Kerviel A, Zhang M, Altan-Bonnet N. 2021. A new infectious unit: extracellular vesicles carrying virus populations. Annu Rev Cell Dev Biol 37:171–197. https://doi.org/10.1146/annurev-cellbio-040621-032416.
8. Kerr CH, Dalwadi U, Scott NE, Yip CK, Foster LJ, Jan E. 2018. Transmission of Cricket paralysis virus via exosome-like vesicles during infection of Drosophila cells. Sci Rep 8:17353. https://doi.org/10.1038/s41598-018-35717-5.
9. Santiana M, Ghosh S, Ho BA, Rajasekaran V, Du WL, Mutsafi Y, De Jesus-Diaz DA, Sosnovtsev SV, Levenson EA, Parra GI, Takvorian PM, Cali A, Bleck C, Vlasova AN, Saif LJ, Patton JT, Lopalco P, Corcelli A, Green KY, Altan-Bonnet N. 2018. Vesicle-cloaked virus clusters are optimal units for inter-organismal viral transmission. Cell Host Microbe 24:208–220.E8. https://doi.org/10.1016/j.chom.2018.07.006.
10. Meckes DG, Jr, Raab-Traub N. 2011. Microvesicles and viral infection. J Virol 85:12844–12854. https://doi.org/10.1128/JVI.05853-11.
11. Hessvik NP, Llorente A. 2018. Current knowledge on exosome biogenesis and release. Cell Mol Life Sci 75:193–208. https://doi.org/10.1007/s00018-017-2595-9.
12. Koles K, Nunnari J, Korkut C, Barria R, Brewer C, Li Y, Leszyk J, Zhang B, Budnik V. 2012. Mechanism of evenness interrupted (Evi)-exosome release at synaptic boutons. J Biol Chem 287:16820–16834. https://doi.org/10.1074/jbc.M112.342667.
13. Théry C, Zitvogel L, Amigorena S. 2002. Exosomes: composition, biogenesis and function. Nat Rev Immunol 2:569–579. https://doi.org/10.1038/nri855.
14. Stenmark H. 2009. Rab GTPases as coordinators of vesicle traffic. Nat Rev Mol Cell Biol 10:513–525. https://doi.org/10.1038/nrm2728.
15. Zhang JH, Chung TD, Oldenburg KR. 1999. A simple statistical parameter for use in evaluation and validation of high throughput screening assays. J Biomol Screen 4:67–73. https://doi.org/10.1177/108705719900400206.
16. Stoorvogel W, Oorschot V, Geuze HJ. 1996. A novel class of clathrin-coated vesicles budding from endosomes. J Cell Biol 132:21–33. https://doi.org/10.1083/jcb.132.1.21.
17. Zhu Y, Drake MT, Kornfeld S. 2001. Adaptor protein 1-dependent clathrin coat assembly on synthetic liposomes and Golgi membranes. Methods Enzymol 329:379–387. https://doi.org/10.1016/s0076-6879(01)29099-5.
18. Robinson MS. 1994. The role of clathrin, adaptors and dynamin in endocytosis. Curr Opin Cell Biol 6:538–544. https://doi.org/10.1016/0955-0674(94)90074-4.
19. Hirst J, Robinson MS. 1998. Clathrin and adaptors. Biochim Biophys Acta 1404:173–193. https://doi.org/10.1016/s0167-4889(98)00056-1.
20. Dell'Angelica EC, Puertollano R, Mullins C, Aguilar RC, Vargas JD, Hartnell LM, Bonifacino JS. 2000. GGAs: a family of ADP ribosylation factor-binding proteins related to adaptors and associated with the Golgi complex. J Cell Biol 149:81–94. https://doi.org/10.1083/jcb.149.1.81.
21. Hirst J, Lui WW, Bright NA, Totty N, Seaman MN, Robinson MS. 2000. A family of proteins with gamma-adaptin and VHS domains that facilitate trafficking between the trans-Golgi network and the vacuole/lysosome. J Cell Biol 149:67–80. https://doi.org/10.1083/jcb.149.1.67.
22. Jackson T. 1998. Transport vesicles: coats of many colours. Curr Biol 8:R609–R612. https://doi.org/10.1016/s0960-9822(98)70388-4.
23. Lipatova Z, Belogortseva N, Zhang XQ, Kim J, Taussig D, Segev N. 2012. Regulation of selective autophagy onset by a Ypt/Rab GTPase module. Proc Natl Acad Sci U S A 109:6981–6986. https://doi.org/10.1073/pnas.1121299109.
24. Morelli E, Ginefra P, Mastrodonato V, Beznoussenko GV, Rusten TE, Bilder D, Stenmark H, Mironov AA, Vaccari T. 2014. Multiple functions of the SNARE protein Snap29 in autophagy, endocytic, and exocytic trafficking during epithelial formation in Drosophila. Autophagy 10:2251–2268. https://doi.org/10.4161/15548627.2014.981913.
25. Chavrier P, Parton RG, Hauri HP, Simons K, Zerial M. 1990. Localization of low molecular weight GTP binding proteins to exocytic and endocytic compartments. Cell 62:317–329. https://doi.org/10.1016/0092-8674(90)90369-p.
26. Gorvel JP, Chavrier P, Zerial M, Gruenberg J. 1991. rab5 controls early endosome fusion in vitro. Cell 64:915–925. https://doi.org/10.1016/0092-8674(91)90316-q.
27. McLauchlan H, Newell J, Morrice N, Osborne A, West M, Smythe E. 1998. A novel role for Rab5-GDI in ligand sequestration into clathrin-coated pits. Curr Biol 8:34–45. https://doi.org/10.1016/s0960-9822(98)70018-1.
28. Feng Y, Press B, Wandinger-Ness A. 1995. Rab 7: an important regulator of late endocytic membrane traffic. J Cell Biol 131:1435–1452. https://doi.org/10.1083/jcb.131.6.1435.
29. Jäger S, Bucci C, Tanida I, Ueno T, Kominami E, Saftig P, Eskelinen EL. 2004. Role for Rab7 in maturation of late autophagic vacuoles. J Cell Sci 117:4837–4848. https://doi.org/10.1242/jcs.01370.
30. Vitelli R, Santillo M, Lattero D, Chiariello M, Bifulco M, Bruni CB, Bucci C. 1997. Role of the small GTPase Rab7 in the late endocytic pathway. J Biol Chem 272:4391–4397. https://doi.org/10.1074/jbc.272.7.4391.
31. Seaman MN. 2012. The retromer complex—endosomal protein recycling and beyond. J Cell Sci 125:4693–4702. https://doi.org/10.1242/jcs.103440.
32. Vogt C, Eickmann M, Diederich S, Moll M, Maisner A. 2005. Endocytosis of the Nipah virus glycoproteins. J Virol 79:3865–3872. https://doi.org/10.1128/JVI.79.6.3865-3872.2005.
33. Gutiérrez-Ortega A, Sánchez-Hernández C, Gómez-García B. 2008. Respiratory syncytial virus glycoproteins uptake occurs through clathrin-mediated endocytosis in a human epithelial cell line. Virol J 5:127. https://doi.org/10.1186/1743-422X-5-127.
34. Gottlieb TA, Gonzalez A, Rizzolo L, Rindler MJ, Adesnik M, Sabatini DD. 1986. Sorting and endocytosis of viral glycoproteins in transfected polarized epithelial cells. J Cell Biol 102:1242–1255. https://doi.org/10.1083/jcb.102.4.1242.
35. Olson JK, Grose C. 1997. Endocytosis and recycling of varicella-zoster virus Fc receptor glycoprotein gE: internalization mediated by a YXXL motif in the cytoplasmic tail. J Virol 71:4042–4054. https://doi.org/10.1128/JVI.71.5.4042-4054.1997.

36. Pfeffer SR. 2017. Rab GTPases: master regulators that establish the secretory and endocytic pathways. Mol Biol Cell 28:712–715. https://doi.org/10.1091/mbc.E16-10-0737.
37. Gillingham AK, Sinka R, Torres IL, Lilley KS, Munro S. 2014. Toward a comprehensive map of the effectors of rab GTPases. Dev Cell 31:358–373. https://doi.org/10.1016/j.devcel.2014.10.007.
38. Ang AL, Taguchi T, Francis S, Folsch H, Murrells LJ, Pypaert M, Warren G, Mellman I. 2004. Recycling endosomes can serve as intermediates during transport from the Golgi to the plasma membrane of MDCK cells. J Cell Biol 167:531–543. https://doi.org/10.1083/jcb.200408165.
39. Park SY, Guo X. 2014. Adaptor protein complexes and intracellular transport. Biosci Rep 34:e00123. https://doi.org/10.1042/BSR20140069.
40. Camidge DR, Pearse BM. 1994. Cloning of Drosophila beta-adaptin and its localization on expression in mammalian cells. J Cell Sci 107:709–718. https://doi.org/10.1242/jcs.107.3.709.
41. Ohno H, Stewart J, Fournier M-C, Bosshart H, Rhee I, Miyatake S, Saito T, Gallusser A, Kirchhausen T, Bonifacino JS. 1995. Interaction of tyrosine-based sorting signals with clathrin-associated proteins. Science 269:1872–1875. https://doi.org/10.1126/science.7569928.
42. Bellec K, Pinot M, Gicquel I, Le Borgne R. 2021. The Clathrin adaptor AP-1 and Stratum act in parallel pathways to control Notch activation in Drosophila sensory organ precursors cells. Development 148:dev191437. https://doi.org/10.1242/dev.191437.
43. Li Z, Blissard GW. 2009. The *Autographa californica* multicapsid nucleopolyhedrovirus (AcMNPV) GP64 protein: analysis of transmembrane (TM) domain length and sequence requirements. J Virol 83:4447–4461. https://doi.org/10.1128/JVI.02252-08.
44. Li Z, Blissard GW. 2008. Functional analysis of the transmembrane (TM) domain of the *Autographa californica* multicapsid nucleopolyhedrovirus GP64 protein: substitution of heterologous TM domains. J Virol 82:3329–3341. https://doi.org/10.1128/JVI.02104-07.
45. Poteryaev D, Datta S, Ackema K, Zerial M, Spang A. 2010. Identification of the switch in early-to-late endosome transition. Cell 141:497–508. https://doi.org/10.1016/j.cell.2010.03.011.
46. Vitale G, Rybin V, Christoforidis S, Thornqvist P, McCaffrey M, Stenmark H, Zerial M. 1998. Distinct Rab-binding domains mediate the interaction of Rabaptin-5 with GTP-bound Rab4 and Rab5. EMBO J 17:1941–1951. https://doi.org/10.1093/emboj/17.7.1941.
47. Farr GA, Hull M, Mellman I, Caplan MJ. 2009. Membrane proteins follow multiple pathways to the basolateral cell surface in polarized epithelial cells. J Cell Biol https://doi.org/10.1083/jcb.200901021.
48. Campbell MJ. 1995. Lipofection reagents prepared by a simple ethanol injection technique. Biotechniques 18:1029–1032.
49. Zhou J, Blissard GW. 2006. Mapping the conformational epitope of a neutralizing antibody (AcV1) directed against the AcMNPV GP64 protein. Virology 352:427–437. https://doi.org/10.1016/j.virol.2006.04.041.
50. Hu Y, Comjean A, Rodiger J, Liu Y, Gao Y, Chung V, Zirin J, Perrimon N, Mohr SE. 2021. FlyRNAi.org-the database of the Drosophila RNAi screening center and transgenic RNAi project: 2021 update. Nucleic Acids Res 49:D908–D915. https://doi.org/10.1093/nar/gkaa936.